11-10-2023

Transport Barriers Influence the Activation of Anti-Tumor Immunity: A Systems Biology Analysis

Mohammad R. Nikmaneshi
Massachusetts General Hospital

James W. Baish
baish@bucknell.edu

Hengbo Zhou
Massachusetts General Hospital

Lance L. Munn
Massachusetts General Hospital/Harvard Medical School

Recommended Citation

Nikmaneshi, M. R., Baish, J. W., Zhou, H., Padera, T. P., Munn, L. L., Transport Barriers Influence the Activation of Anti-Tumor Immunity: A Systems Biology Analysis. Adv. Sci. 2023, 2304076. https://doi.org/10.1002/advs.202304076

ADVANCED SCIENCE Open Access
www.advancedscience.com

Transport Barriers Influence the Activation of Anti-Tumor Immunity: A Systems Biology Analysis

*Mohammad R. Nikmaneshi, James W. Baish, Hengbo Zhou, Timothy P. Padera, and Lance L. Munn**

Effective anti-cancer immune responses require activation of one or more naïve T cells. If the correct naïve T cell encounters its cognate antigen presented by an antigen presenting cell, then the T cell can activate and proliferate. Here, mathematical modeling is used to explore the possibility that immune activation in lymph nodes is a rate-limiting step in anti-cancer immunity and can affect response rates to immune checkpoint therapy. The model provides a mechanistic framework for optimizing cancer immunotherapy and developing testable solutions to unleash anti-tumor immune responses for more patients with cancer. The results show that antigen production rate and trafficking of naïve T cells into the lymph nodes are key parameters and that treatments designed to enhance tumor antigen production can improve immune checkpoint therapies. The model underscores the potential of radiation therapy in augmenting tumor immunogenicity and neoantigen production for improved ICB therapy, while emphasizing the need for careful consideration in cases where antigen levels are already sufficient to avoid compromising the immune response.

1. Introduction

Immune checkpoint blockers (ICBs) have transformed cancer treatment by inhibiting the interactions between receptor-ligand pairs that limit the immune response—so-called immune checkpoints, including CTLA-4 and PD-1/PD-L1.[1,2] ICB therapy has produced durable responses in patients with advanced melanoma and non-small cell lung cancer, among other cancers.[3,4] Although extremely encouraging, not all patients benefit, and a better understanding of immune function and checkpoint control is needed to improve outcomes.[5]

Many processes are involved in initiating and sustaining anti-cancer immune responses, including the generation of antigen and its presentation on major histocompatibility complex (MHC) molecules. A less-studied and potentially critical step is the physical colocalization of cancer specific naïve T-cells (nTcells) with antigen presenting cells (APCs) displaying their cognate antigen. This step is necessary for the generation of anti-tumor effector T cells and is thought to take place primarily in lymph nodes.[6–9] T-cell activation occurs when an nT-cell encounters an APC (e.g., dendritic cell) displaying antigen on MHC molecules that the nT-cell can specifically recognize via its T-cell receptor. This T-cell receptor/MHC/cognate antigen interaction (signal 1) needs to also have co-stimulatory signaling between the nT-cell and APC (signal 2) to induce the activation of effector T-cell responses.

The co-localization of the APC, nT-cell and cognate antigen is facilitated by the lymphatic system. As initial lymphatic vessels absorb interstitial fluid, they also collect antigen and APCs. Both are then concentrated in lymph nodes, creating a target-rich environment for nT-cells to surveil.[10]

Although there are $\approx 10^{11}$ nT-cells in humans, each clone has unique specificity.[11] Because humans need to harbor a large variety of nT-cell clones to protect against a diversity of potential pathogens, there are few nT-cells specific for any given antigen.[12–15] This may limit immune activation, which requires the colocalization of the correct nT-cell with sufficient cognate antigen.[11] For activation of anti-tumor immunity, one of the few nT-cells capable of recognizing tumor antigen needs to visit a lymph node where tumor antigen has accumulated and the microenvironment is not already immune suppressive. Cancer-specific nT-cells execute a random search throughout the body, sampling secondary lymphoid organs. Thus, a nT-cell may circulate many times before finding a lymph node, and many more times before entering a lymph node with sufficient cognate antigen. As there are multiple parallel paths through the circulation that an nT-cell could take, it becomes a probabilistic process to bring a cognate nT-cell to a lymph node draining the tumor.[16] Once activated, the expanding population of clonal T cells leaves the node, enters the blood, and travels through the blood

M. R. Nikmaneshi, H. Zhou, T. P. Padera, L. L. Munn
Department of Radiation Oncology
Massachusetts General Hospital and Harvard Medical School
Boston, MA 02114, USA
E-mail: munn@steele.mgh.harvard.edu
J. W. Baish
Biomedical Engineering
Bucknell University
Lewisburg, PA 17837, USA

The ORCID identification number(s) for the author(s) of this article can be found under https://doi.org/10.1002/advs.202304076

DOI: 10.1002/advs.202304076

circulation. After adhesion to blood vessel endothelium and extravasation, they can enter the target tissue and kill antigen-bearing cells unless checkpoint molecules (e.g., PD-1) prevent it (which can result in anergy or "exhaustion" of the effector T-cell).

The probabilistic nature of nT-cell sampling of lymph nodes makes it challenging to predict when the nT-cell will arrive in a tumor draining lymph node (TDLN)—and whether there will be sufficient antigen when it arrives. Activation of nT-cells also requires that the LN with antigen is not immunosuppressed when the cognate nT-cell arrives. Such stochastic processes may explain why previously-validated biomarkers do not predict with certainty the response of a given patient to ICB therapy.[17,18] Randomness may also explain why genetically identical mice can have different tumor responses to the same ICB therapy.[19,20] For example, ≈40% of mice with identical E0771 tumors growing in the mammary fat pad respond to anti-PD-1 therapy, while tumors in the remaining 60% of mice continue to grow like controls.[20] Because these mice are genetically identical, the binary response suggests that there is a stochastic process that leads to immune activation in only some mice. Furthermore, when two tumors are grown in different mammary fat pads in the same mouse, they either both respond to the ICB or they both continue to grow like control tumors.[20] This suggests that the "switch" that is activated in the responders operates at the systemic level rather than locally within a tumor. Interestingly, rechallenging long-term surviving mice with the original cancer cells or a tumor harvested from a non-responding mouse results in the rejection of the tumor.[20] This indicates that the successful ICB response is not due to the creation of unique neoantigens in the responders, but rather a systemic-level activation event that is able to recognize the original tumor antigens.

Here, we explore the hypothesis that anti-cancer immune responses are limited by the frequency of encounters between naïve T cells and appropriate antigen/APCs using a pharmacokinetic-based systems biology computational model. Such models represent each component of the system and how those components interact with one another over several length scales.[21–30] There is a rich literature of pharmacokinetic-pharmacodynamic (PKPD) or quantitative systems pharmacology (QSP) models of the circulation of therapeutic agents, antigens, and immune cells in the blood and lymph.[31–34] The simplest of these consider only a single tumor and a single lymph node, while more detailed models include several additional organs. In addition, other models focus on the pumping dynamics of individual (or small networks of) lymphatic vessels that are responsible for lymph flow between the tumor (and peripheral tissues) and lymph nodes.[35–41]

The whole-body model includes compartments representing the tumor, lung, liver, spleen, intestine, brain, kidney, skin, bone, muscle, and heart (**Figure 1**). Blood flow follows anatomically-accurate pathways and is distributed to the various organs via branches in the arterial tree, according to flow volumes reported in the literature.[26,30,42] Each compartment of the model contains a sub-compartment for the organ and another sub-compartment representing the lymph node(s) draining that organ. Each sub-compartment receives a fraction of the blood flow entering that organ, and a fraction of interstitial fluid collected from the tissue is assumed to flow into the draining lymph nodes (LNs). Lymph exits the LNs and enters the converging network of lymphatic vessels to return to the venous circulation.

The model simulates immune responses as follows. We calculate tumor growth, antigen production, and the accumulation of antigen in various LNs. Antigen produced by the tumor either convects or is carried by APCs into lymphatic vessels and then accumulates in the tumor draining lymph node (TDLN). A fraction of the antigen (Table S1 of the supplementary material) also passes through the initial lymph node to arrive in additional LNs or return to the blood circulation. This simulates the bypass of antigen through the LN subcapsular sinus.[43]

For the circulation of the naïve T cells, we use a stochastic model to keep track of their location as they circulate through the blood stream, visiting various tissues and LNs during each pass through the blood system (see Figure S8, Supporting Information). At bifurcations, the direction of the naïve T cell is determined by a random function weighted by the relative flow rates in the daughter branches. The residence time in each lymph node is 10 h, and the residence times for the other organs are listed in Table S1 (Supporting Information).[44,45] We assume that any nT-cell that enters the blood system of a lymph node will extravasate into the node via HECs. Once in the node, we use a threshold to determine whether the nT-cell becomes activated based on the local level of antigen in that node.

If an nT-cell is activated, it becomes a cytotoxic T lymphocyte (CTL) and starts to proliferate in the node. Exit of the CTLs from the node is determined by a Heaviside function based on a limited capacity of the LN to contain CTLs. CTLs that exit the LN enter the systemic circulation (through lymphatic drainage). They bind to activated tumor blood vessels and extravasate into the tumor tissue. Once they enter the tumor, they kill cancer cells if the immune checkpoint status is sufficiently permissive.

In the simulations, tumor volume is influenced by intrinsic growth of cancer cells and cancer cell killing by T cells or radiation therapy. T cell activation is affected by antigen accumulation in the lymph nodes and the antigen immunogenicity, which is related to the activation threshold.

2. Results and Discussion

To demonstrate the key features of the model, we first simulated a single patient with a tumor growing in the breast. Note that the location of the primary tumor affects the dissemination of antigen to various lymph nodes, so results will be somewhat affected by the site of tumor initiation. As the tumor grows (**Figure 2**A), it begins to release antigen into the surrounding tissue, which is collected by lymphatic vessels and passed to the draining lymph node basin (represented by a single node for model simplicity). Some antigen can also bypass the tumor draining lymph node, entering the systemic circulation where it is diluted, but can potentially accumulate in other nodes more distant from the tumor (Figure 2B). The model assumes that no activation can take place until a threshold level of antigen is present in a node (dashed line, Figure 2B). At the same time, a naïve T cell circulates through the blood system, entering various LNs in a random search for antigen (Figure 2C). If it enters a LN with sufficient antigen, it becomes activated and starts to proliferate. The resulting effector T cells exit the node, infiltrate the tumor, and begin killing cancer cells (Figure 2D).

There are two characteristic time delays associated with the model—the time it takes for sufficient antigen to accumulate in

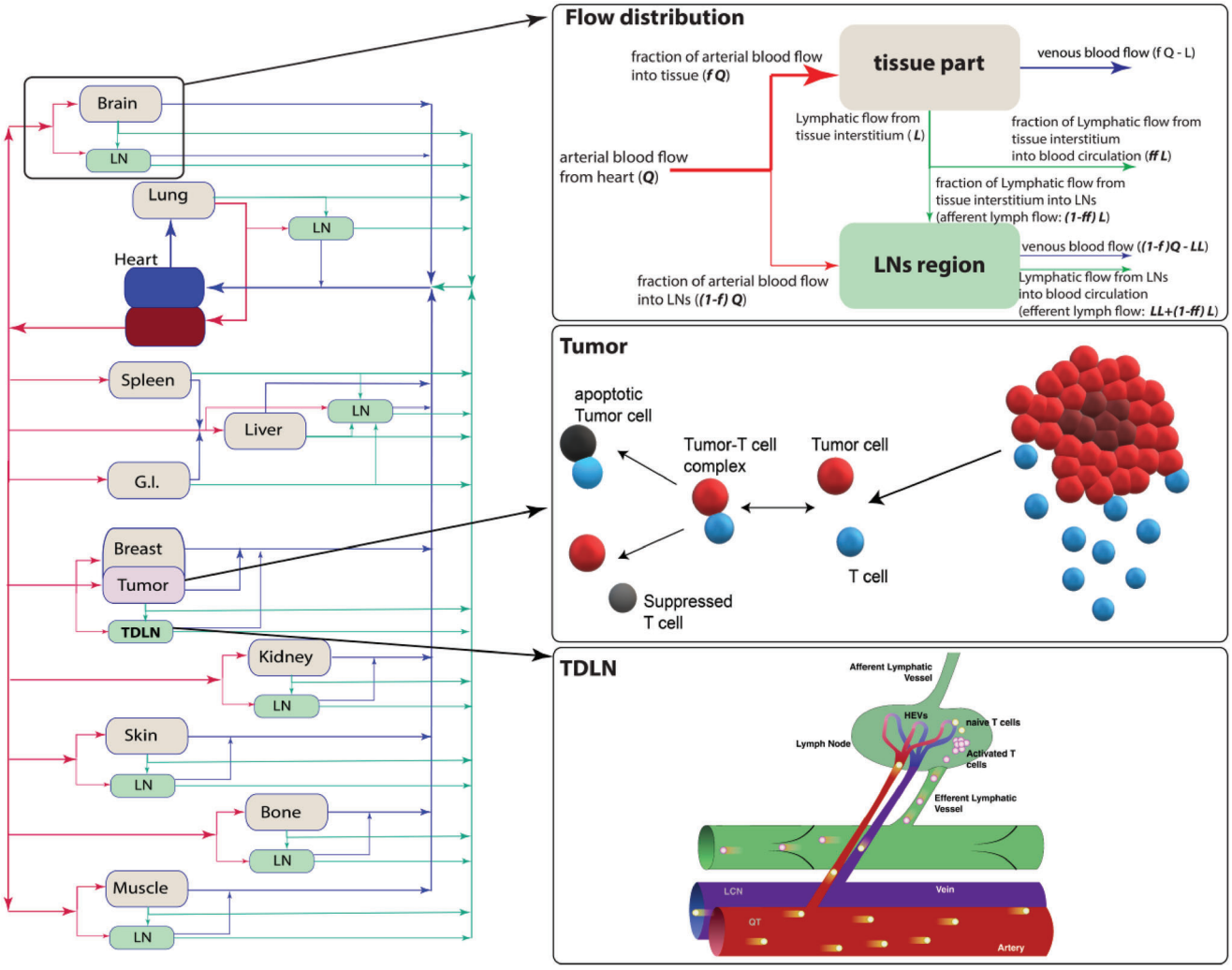

Figure 1. Schematics of the tumor-immune microenvironments and the free diagram of the compartmental PKPD model. The arrows of blood and lymphatic flows are scaled corresponding with flow rates. Trafficking of T cells occurs through the systemic blood circulation, lymph node and exit through the efferent lymphatic vessel. In the flow distribution panel, Q is blood flow, L is lymphatic flow collected from tissue interstitium (afferent lymph), and LL is lymphatic flow collected from LN interstitium (efferent lymph). f is the fraction of blood flow into an organ tissue and ff is the fraction of tissue lymphatic flow, which is directly released into the systematic lymphatic flow. Thus, $(1\text{-}f)Q$ is the fractional flow rate of blood that enters a lymph node (LN-FFR), and $(1\text{-}ff)L$ is the fraction of tissue lymphatic flow that enters a lymph node.

a given node, t_a, and the time it takes for a naïve T cell to find the node, once it has sufficient antigen, t_T. The first is deterministic, and the second is stochastic. They are also not independent, as t_T depends on the accumulation rate of antigen and is relative to the time that antigen surpasses the threshold. In this particular simulation, antigen surpasses the threshold in the TDLN on day 5, and a nT-cell visits that node 1 day later. This results in an anti-tumor immune response that escalates starting at day 6 and decreases tumor volume by ≈20% between days 12 and 14.

2.1. Blood Flow Partitioning into Lymph Nodes (LNs) Affects Tumor-Immune Response

One of the key events in immune surveillance is the entry of nT-cells into the lymph node arterial supply. In the model, this step requires specification of the fractional flow rate of blood that enters a lymph node (LN-FFR; $(1\text{-}f)Q$ in the Flow distribution panel of Figure 1). Because the experimental data are limited, we simulated a range of fractional flow rates into the LN, so that 0.5%, 1%, 5%, or 10% of nT-cells were diverted to the LN vasculature in each organ.[46] This is in the range of reported values as well as estimates based on relative tissue volumes (see Figure S1, Supporting Information). Another critical unknown parameter is the rate of production of antigen by the tumor. To examine the importance of antigen production, we simulated tumors with low, medium, and high antigen production rates.

In the simulations, when sufficient antigen is encountered by a naïve T cell within a lymph node, the T cell becomes activated. We examined this process for cancer patients with low, medium, and high production rates of tumor antigen. Because of the stochastic nature of the model, we simulated 100 tumors in each group,

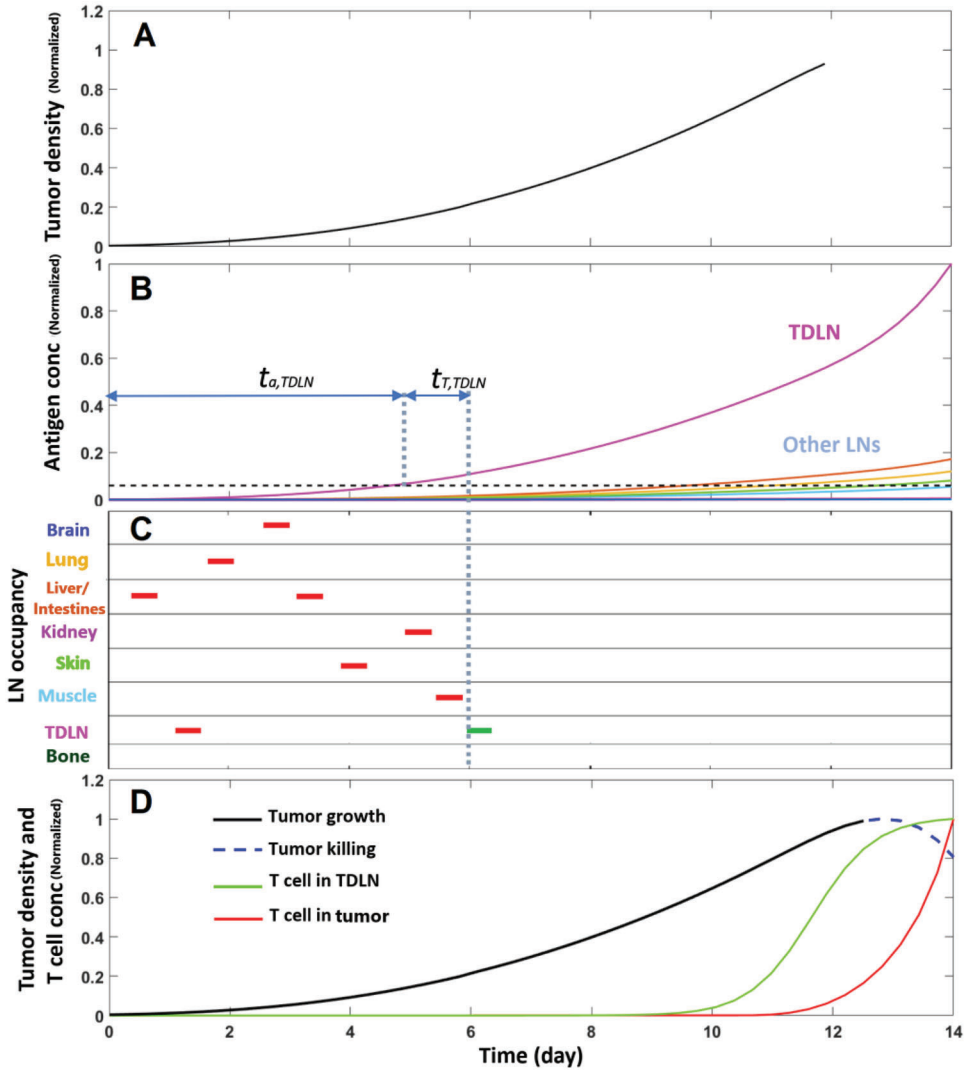

Figure 2. Simulating activation of anti-tumor immunity. Shown are results from a single patient. A) Tumor growth normalized by maximum value of tumor density. B) tumor-induced antigen accumulation in different lymph nodes, normalized by the maximum value of antigen concentration. C) stochastic circulation of naïve T cells in different lymph nodes. The colored lines show different LN sites and bars represent resident times of a naïve T cell in each LN. The liver/intestines LN represents abdominal LNs (LN_Abd). D) tumor growth, tumor killing by effector T cells, T cell accumulation in the TDLN and tumor—the values are normalized to the maximum value in each case.

which we followed for two weeks (**Figure 3**A). The results show that increasing the fraction of nT-cells that exit the blood circulation to enter the vasculature of a lymph node (LN-FFR) dramatically enhances the probability of activation of nT-cells in patients with high and medium—but not low—antigen production. The response in patients with high antigen production is even more sensitive to LN-FFR than that in medium antigen patients.

We can also record the time at which activation occurs (Figure 3B). Increasing LN-FFR can considerably decrease the time required for activation ($t_a + t_T$) in patients with high antigen production rate, but it has less impact on the time of patients with medium antigen production rate.

We then plotted the cumulative event probabilities for activation of the T cells for high (Figure 3C) and medium (Figure 3D) antigen production rates. These results show that increasing LN-FFR or antigen production rate can decrease the time needed for T cell activation.

We next examined the ability of the activated T cells to reduce tumor volume. To simplify the biology, we assume that immune checkpoint inhibition is nearly complete and T cell exhaustion is minimal (relative rate constants = 0.99 and 0.01, respectively). Consequently, once the effector T cells circulate to the tumor, they are likely to initiate a sustained anti-tumor response. With these assumptions, the key parameters that determine tumor eradication are the tumor growth rate and time of activation of the T cells. To examine tumor size reduction in the patients who had T cell activation, we calculated the relative tumor size reduction (TSR) (**Figure 4**).

Considering only those patients with successful T cell activation in the 2-week period, those with high antigen production

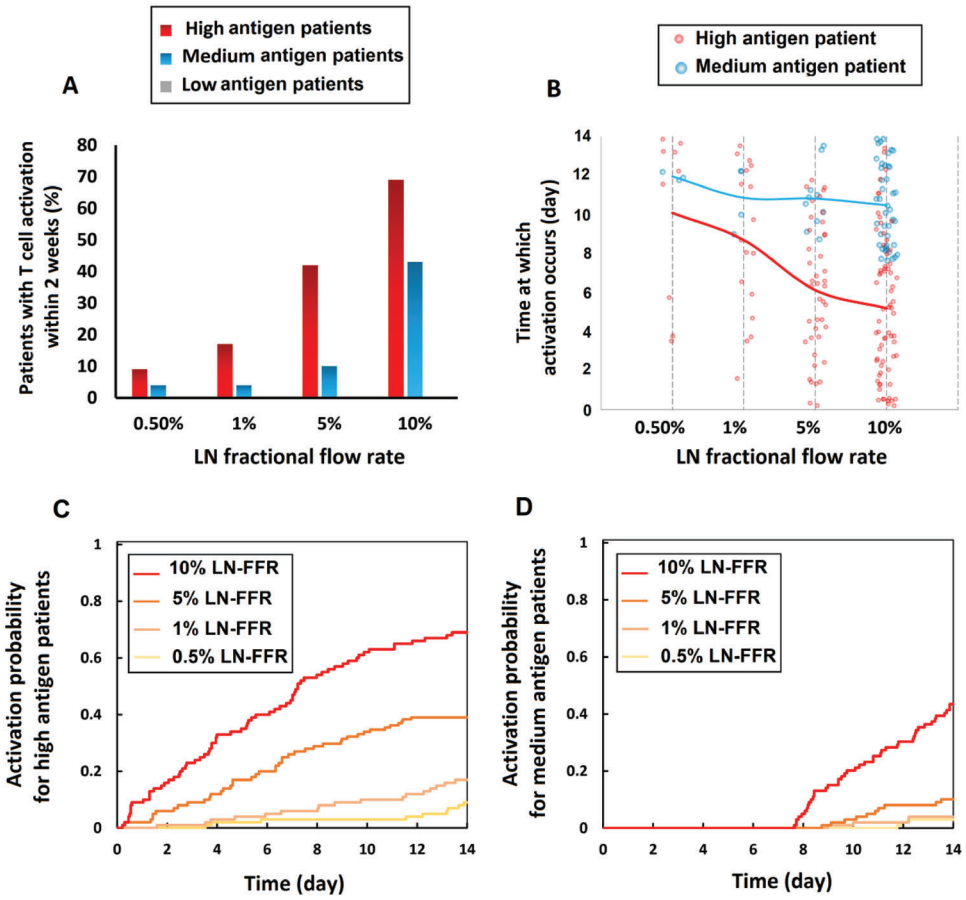

Figure 3. Effects of partitioning of nT-cells into the LN circulation and antigen production rate on T cell activation. A) The probability of a single T cell activation event within 2 weeks of simulation for cancer patients with low, medium, and high tumor-induced antigen rates under different LN fractional flow rates; 0.5%, 1%, 5%, and 10% of the total blood flow rate feeding each organ. B) Time elapsed before T cell activation in patients with high antigen rate (red circles) and medium antigen rate (blue circles); the averages are given by the red and blue lines, respectively. C) Cumulative event probability for T cell activation in high antigen patients, D) Cumulative event probability for T cell activation in medium antigen patients.

had a much greater probability of tumor eradication than those with medium antigen production, due to the earlier activation of immunity. Data points between 0 and 1 indicate the fractional reduction in tumor volume relative to unchecked growth measured at the 2 week time point. These numbers are in the range reported for clinical treatment of melanoma and small cell lung cancer.[47–50] Increasing the LN-FFR has a strong effect on the high antigen patients, but less effect on medium antigen production.

These results can also be visualized by plotting the tumor size as a function of time for each patient (**Figure 5**). As explained in the supplementary material (Figure S2, Supporting Information), we used a simplified version of our model to estimate a threshold time for T cell activation. If the tumor is small enough when the effector T cells arrive, they can eliminate it; otherwise, tumor growth can out-pace immune killing (Figure S2, Supporting Information). In this analysis, the critical time for nT-cell activation is 4.62 days, and activation at this time leads to a tumor size reduction of 0.7 at the two-week time point. If T cell activation takes longer than the threshold time, tumor growth outpaces the immune response in two weeks, and the tumor is not eradicated (designated "non-responder" with TSR < 0.7). Earlier activation, before the threshold time, results in tumor clearance ("responder" with TSR within 0.7–1; see Figure S2, Supporting Information). In Figure 5, the plots show the time when antitumor killing by the T cells is initiated and the time course of tumor shrinkage (dashed lines). For example, for the high antigen tumors and the case of 10% LN-FFR, 69/100 patients had T cell activation within the two-week period, and 37 of these occurred sufficiently early to decrease the tumor size by >70% (TSR range = 0.7–1, according to Figures 4 and 5, "High antigen patients, 10% LN fractional flow rate"). As expected, higher tumor antigen production rates increase the activation probability, and this is further enhanced by increasing LN-FFR.

2.2. Can LN-Sparing Radiation Therapy Enhance Anti-Tumor Immunity?

We next examined how radiation therapy applied to the tumor and/or TDLN affects the activation of the immune response. There is evidence that radiation therapy can help generate neoantigens, thus synergizing with ICB therapies.[32,51,52] On the other hand, it is thought that irradiation of a reactive TDLN

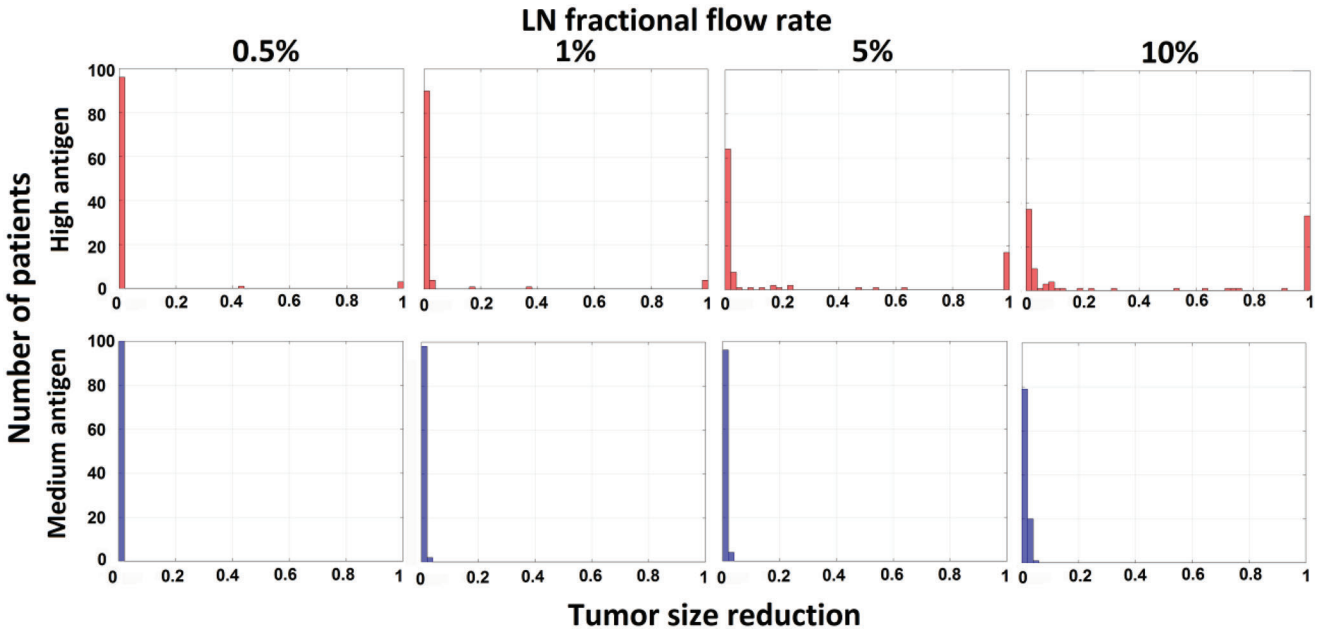

Figure 4. Tumor size reduction (TSR) ratio in response to activation of natural immunity with high (top) and medium (bottom) production rates of tumor-induced antigen under different LN-FFR. A TSR of zero indicates no response, while TSR = 1 indicates tumor eradication.

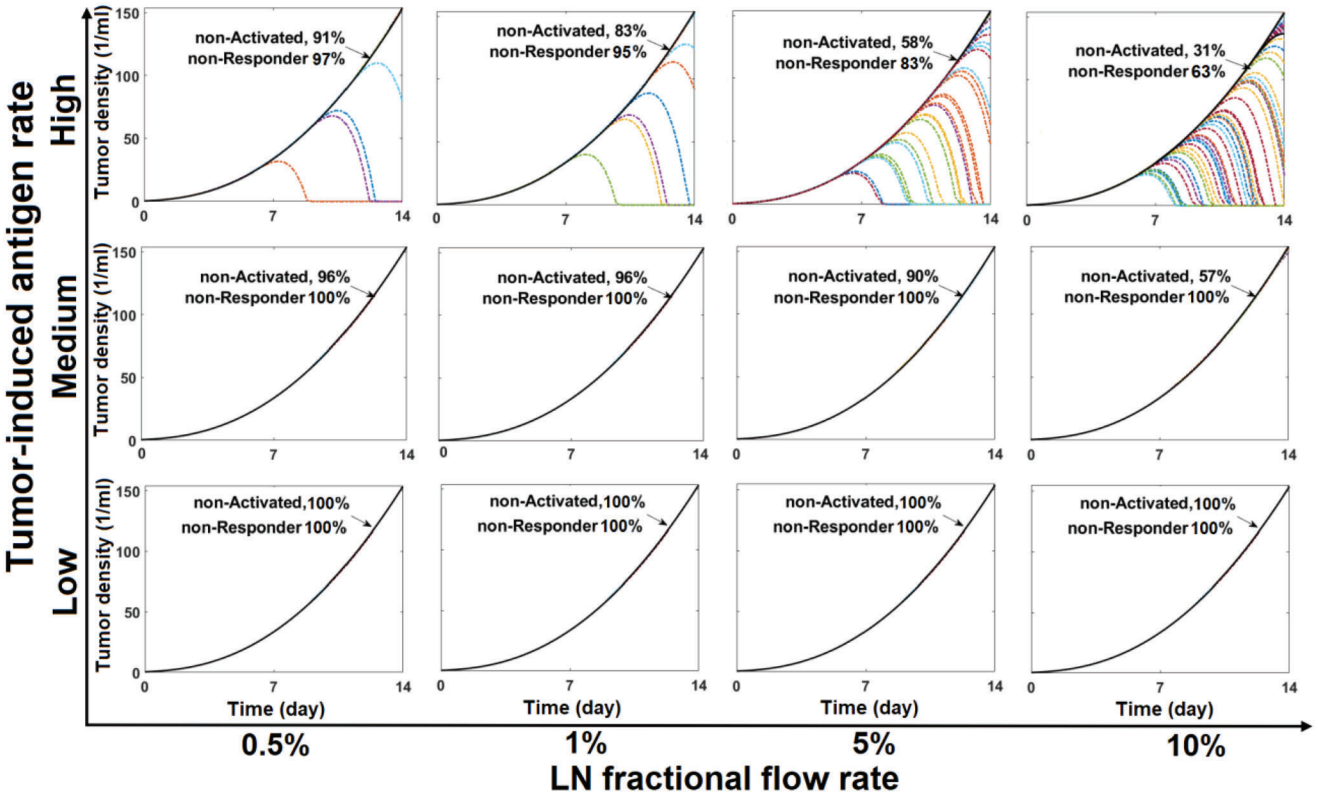

Figure 5. Effects of tumor antigen production rate and LN fractional flow rate (LN-FFR) on T cell activation and tumor elimination. Each result shows tumor growth and the probabilities of non-activated and non-responder immunity of 100 cancer patients for two weeks. The black solid-line shows non-responder patients and colored dot-dash lines show individual patients with tumor reduction due to T-cell killing.

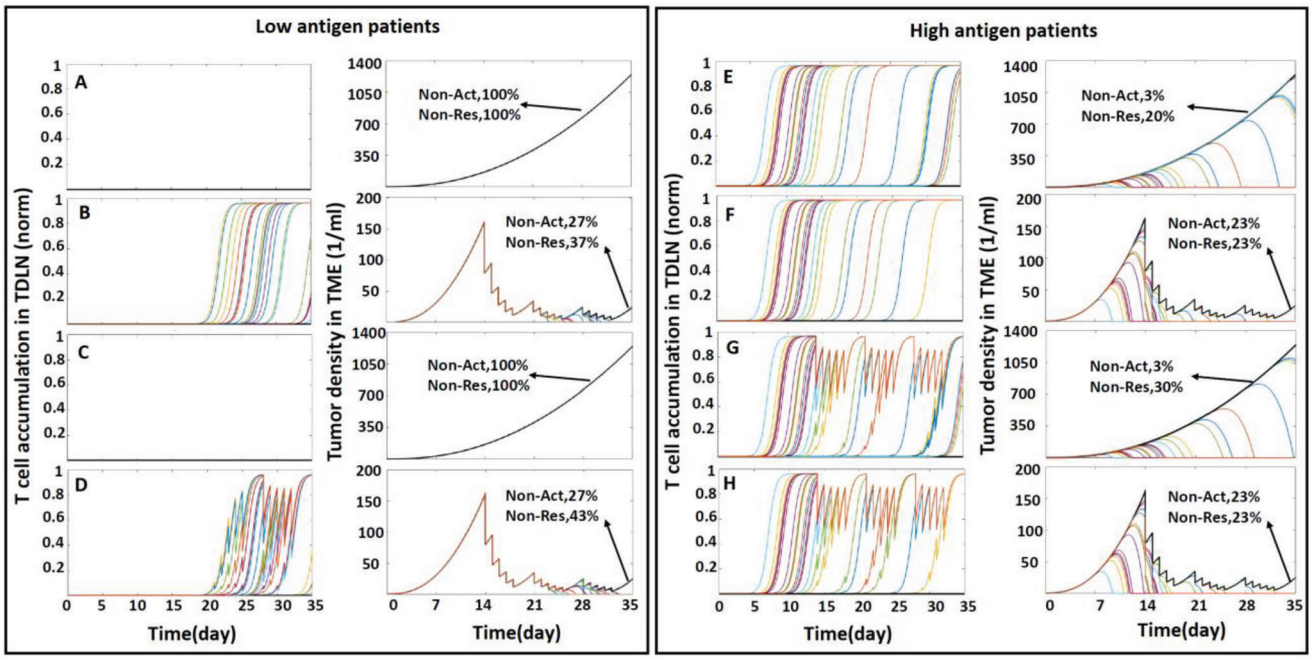

Figure 6. Effect of radiotherapy on tumor-immune response in low and high antigen patients with LN-FFR equal to 10%. Thirty cases were simulated for each condition. RT starts on day 14, with daily dose of 2 Gy, except two days (weekend), administered over three weeks. A) Non-irradiated low antigen patients. B) RT on tumor of low antigen patients. C) radiation applied to the TDLN of low antigen patients. D) RT on tumor and TDLN of low antigen patients. E) non-irradiated high antigen patients. F) RT on tumor of high antigen patients. G) RT to TDLN of high antigen patients. H) RT on tumor and TDLN of high antigen patient. The black line shows patients in which T-cell activation does not occur. Colored lines show the T cell accumulation and tumor size in individual patients who have T-cell activation. Tumor size and T cell numbers are stochastically increased by activation and are decreased by radiation treatment.

can interrupt immune activation.[53] To examine this with our model, we simulated irradiation of the tumor, which we assume kills cancer cells, any resident proliferating T cells and endothelial cells, and also increases effective antigen production rate due to antigen shedding from the irradiated cells. We also simulated irradiation of the TDLN, which we assume damages proliferating, activated T cells.

We simulated a 3-week radiotherapy (RT) schedule, restricting the treatment to the tumor, the TDLN, or both. This was repeated for patients with low and high baseline antigen production to investigate the effects of RT on T cell activation and tumor killing. We assume that the RT doses are applied daily for five days each week. In this study, the TSR ratio is calculated based on the size of the non-irradiated tumor at day 35 for RT applied to only the TDLN. For cases where the tumor is irradiated (with or without LN exposure), TSR is relative to the control case where there is no immune activation and tumor growth for 35 days.

The results of T cell accumulation in the TDLN and tumor size are shown in **Figure 6** for low and high antigen producing tumors. For the low antigen group, T cell activation only happens when RT is applied on the tumor or the tumor+TDLN (Figure 6A–D). Note that here, we assume that lymph node irradiation does not interfere with T cell activation—only proliferation/viability after activation. In both cases, 73% of patients have T cell activation within the 35-day period (Figure 6B,D). The resulting immune response, combined with killing due to the radiation, leads to TSR-classified responders in 63% and 57% of the tumor only and tumor+TDLN groups, respectively (Figure 6B,D).

For the high antigen group with no irradiation, 97% have activation within 35 days, and 80% are classified as responders (Figure 6E). Irradiating the tumor alone reduces both the T cell activation and responder probabilities to 77% (Figure 6F). Irradiation of the TDLN affects the responder probability more than the activation of T cells: with TDLN irradiation alone, 97% of patients have T cell activation, but only 70% have sufficient tumor killing by day 35 to fall into the "responder" category (Figure 6G). Interestingly, in these patients with high baseline antigen production, irradiating the TDLN with the tumor does not change the outcomes compared with irradiation of the tumor alone (Figure 6F,H).

The results of T-cell accumulation in the TDLN for low and high antigen patients receiving RT to the tumor or TDLN or both are also shown in Figure 6. These results suggest that antigen production rate can be used to guide the appropriate timing of ICB therapy. Assuming that ICB therapy primarily affects killing at the tumor site, and not T cell activation in the nodes, it would be best to apply ICB drugs during the time window when T cell activation is most likely to be happening. This would allow the mobilized effector T cell to most efficiently kill the tumor. For low antigen patients irradiated on the tumor or on the tumor and TDLN, the optimal window for ICB would be days 19–30 (Figure 6B,D). The model predicts that patients with low antigen production and no tumor irradiation do not have T cell activation,

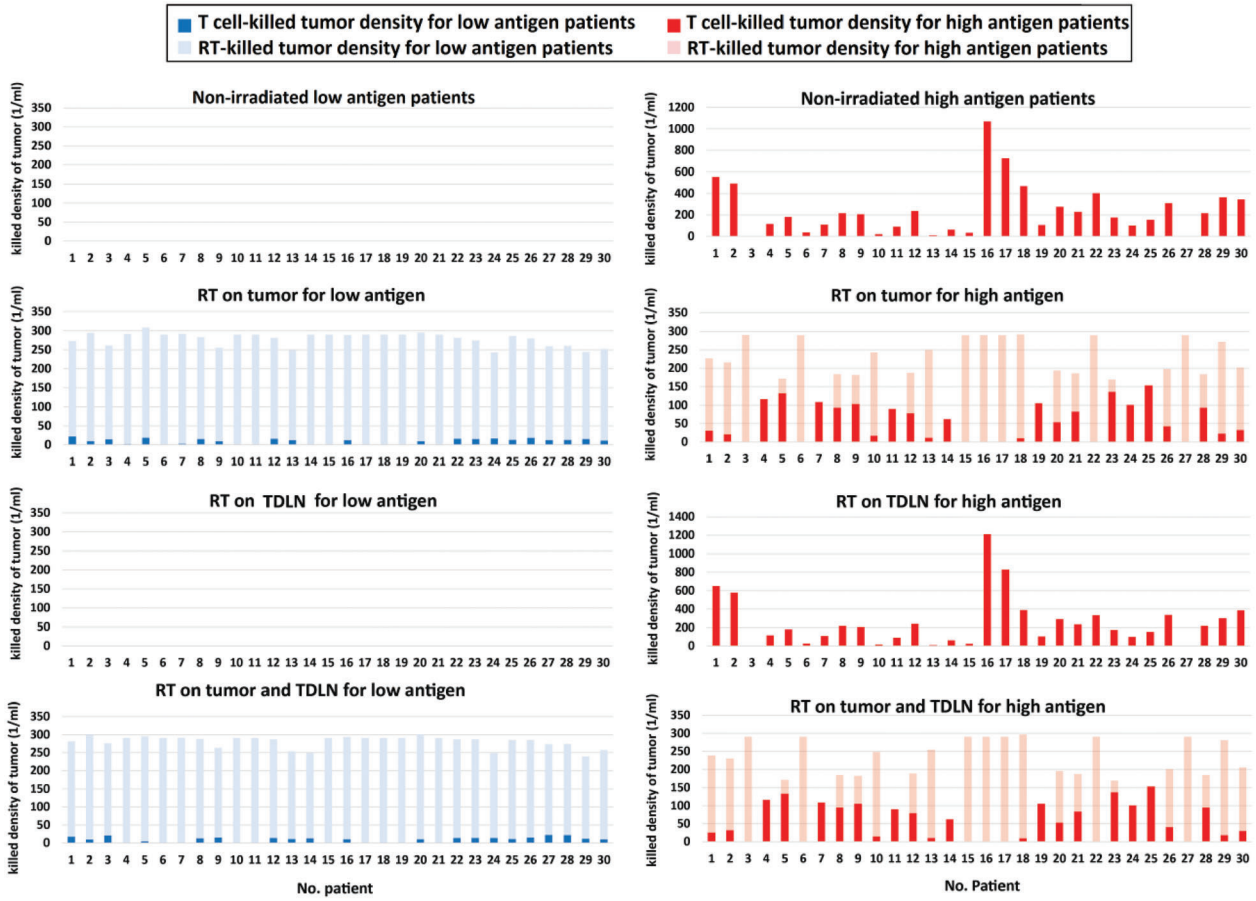

Figure 7. Comparison of the fractions of cancer cells killed by radiation therapy ("RT-killed") and by the immune response ("T-cell killed"). Results for 30 independent simulations are shown for low (blue, left) and high (red, right) antigen producing cases. RT was applied to the tumor only, to the TDLN only, or to both tumor and TDLN.

and thus would not benefit from ICB therapy (Figure 6A,C). In contrast, most of the patients with high antigen production with or without RT have T cell activation and can benefit from ICB treatment starting as early as day 5. The results show that tumor irradiation in these patients with high baseline antigen production does not enhance T cell activation. To examine the effect of LN-FFR on immunity and radiation response, we recalculated the results of Figure 6 for LN-FFRs of 5%, 1%, and 0.5%. These results are shown in Figures S3–S5 (Supporting Information). To elucidate the importance of ICB for the patients with activated immune responses (Figure 6E), we compared RT applied to the tumor, ICB therapy and their combination for the high antigen patients with LN-FFR equal to 10%. The results are shown in Figure S6 (Supporting Information).

To quantitatively investigate the importance of RT for treatment of low and high antigen patients, we quantified the contributions of the anti-tumor immune response and the radiation-induced cytotoxicity on tumor size reduction separately (**Figure 7**). For high antigen patients the ratio of contributions to tumor killing due to RT and T cells have the same order of magnitude (Figure 7). However, for low antigen patients, the RT has a larger impact on tumor killing compared with the T cell mediated anti-tumor immunity. In this case, RT is responsible for between 92 to 100% of the cell death, while the T cells are responsible for between 0 to 8% cancer cell killing (Figure 7). These results reinforce the result that low antigen patients may receive significant benefits from RT. However, high antigen producing tumors can be eradicated by immune response with or without RT. In some high antigen patients with delayed T cell activation, and thus higher T cell-killed fraction (No. patient 15–17), RT of the tumor will reduce the antigen source and delay systematic circulation of antigen, which will stop T cell activation. Therefore, for high antigen patients, the application of radiation to the tumor may be counter-productive.

3. Conclusion

Colocalization of naïve T cells with tumor antigen is a necessary but potentially inefficient step in anti-tumor immunity. Before an immune response can be mounted against a tumor, T cells that recognize tumor antigen have to be activated and expanded. Although much research has focused on therapeutic modulation of immune checkpoint (IC) programs, relatively little is known about the systemic events the lead to T cell activation and their accumulation in the tumor. Here, we developed a model that simulates tumor growth, antigen production, the accumulation

of antigen in lymph nodes and the trafficking of T cells, the IC mechanism for tumor-immune interactions, and the implicit and explicit effects of radiotherapy on cancer clearance through the immunogenic and non-immunogenic mechanisms. The simulations suggest that T cell activation depends strongly on two processes: the partitioning of T cells into lymph nodes as they circulate through the blood and the production rate of antigen by the tumor. Increasing the fraction of nT-cells entering a lymph node significantly enhances the probability of activation in patients with high and medium antigen production rates and can considerably decrease the time required for activation in patients with high antigen production. Increasing LN-FFR or antigen production can decrease the time needed for T cell activation.

The model has several limitations that should be considered as we interpret the results. For example, we use a simplified anatomy, with the multiple LNs associated with each organ "lumped" together into a representative node for that organ. We also have not included mechanisms of T cell retention in the LNs due to immune status or antigen level, which probably affect residence times. Furthermore, we did not explicitly consider T cell activation in the spleen, although this is likely justified, as blood-borne antigen is highly diluted and accumulates in lower levels in the spleen compared with the draining lymph nodes. Note also that, in addition to the transport limitations studied here, defects in antigen processing and presentation machinery and the presence of immunosuppressive cell types can also determine the effectiveness of an anti-tumor immune response. Other limitations are that the time course analyzed is limited, and the dynamics of T cell activation and tumor killing are necessarily simplified. Finally, we assume that immune checkpoint blockade is persistent and nearly complete, and the exhaustion rate of effector T cells is very small.[45,54,55] These assumptions simplified the analysis, allowing us to focus on the systemic transport limitations rather than biological impediments to T cell activation and killing. Where significant T cell exhaustion occurs, a continued antitumor immune response would require the activation of additional nT-cell clones as previous effector T cells become ineffective.[41,56] This process encompasses complex dynamics that are largely unknown, but that would be expected to amplify the importance of the stochastic processes explored here.

The simulations highlight the importance of tumor draining lymph nodes for the initiation of tumor immunity. Activation of nT-cells in TDLNs can be compromised for various reasons, including inhibition by cytokines produced in the tumor and physical removal of the LN(s) during cancer surgery. Hence, we also examined the anti-tumor immune response following TDLN removal (Figure S7, Supporting Information). Mathematical removal of the TDLN results in a delay in T cell activation because antigen accumulation in other lymph nodes is slower, and activation is consequently delayed compared with activation in the TDLN. Clinically, elective nodal irradiation, in which the tumor draining lymph nodes are targeted by the radiation field, is a common strategy designed to minimize regional recurrence. However, there is concern that the tumor draining lymph nodes should be spared from radiation therapy, as these are the sites of immune cell activation and expansion.[57,58] Consistent with this, our results suggest that nodal irradiation can be counterproductive in patients with tumors that have low antigen production, because of toxic effects on proliferating T cells in the active nodes. This effect is less prominent when tumor antigen production is high because nT-cell activation is more frequent, and not rate-limiting. This agrees with clinical and experimental evidence showing that lymph node irradiation increases local and metastatic tumor growth, decreases the systemic immune response, and decreases antigen-specific T cells and epitope spreading.[57]

In addition to concerns about LN irradiation, there are emerging questions about the appropriate use of therapies for killing cancer cells and enhancing antigen/neoantigen production in the context of immunotherapy. Specifically, it has been shown that radiation therapy applied to cancer cells can enhance tumor immunogenicity and creation of neoantigens, thus improving the response to ICB therapy.[59] Our model supports this, predicting that irradiation of the tumor can enhance immunotherapy. However, it suggests that radiation should be considered carefully: radiation applied to the tumor in patients where the antigen level is already sufficient for successful ICB therapy may decrease the source of antigen, potentially abrogating the immune response in these tumors. The simulations also suggest that the timing of ICB therapy should be guided by the antigen production rate and the time window when T cell activation is most likely to occur.

Supporting Information

Supporting Information is available from the Wiley Online Library or from the author.

Acknowledgements

This work was supported by the NIA R21AG072205, the NCI R01CA214913 and R01CA284372 (T.P.P.), the NHLBI R01HL128168 and the NCI R01CA284603 (L.L.M., T.P.P., J.W.B.), the NCI R01CA2044949 and U01CA261842 (L.L.M.) and the Rullo Family MGH Research Scholar Award from the Massachusetts General Hospital Research Institute (T.P.P.).

Conflict of Interest

L.L.M. is a consultant for SimBiosys and receives equity from Bayer.

Data Availability Statement

The data that support the findings of this study are available in the supplementary material of this article.

Keywords

anti-tumor immunity, immune activation, radiotherapy, T cell trafficking, tumor-induced antigen

Received: June 20, 2023
Revised: October 7, 2023
Published online:

[1] M. K. Callahan, J. D. Wolchok, *Semin. Oncol.* **2015**, *42*, 573.

[2] M. A. Postow, M. K. Callahan, J. D. Wolchok, *J. Clin. Oncol.* **2015**, *33*, 1974.
[3] K. Sanchez, D. Page, H. L. McArthur, *Curr. Probl. Cancer* **2016**, *40*, 151.
[4] K. M. Mahoney, P. D. Rennert, G. J. Freeman, *Nat. Rev. Drug Discovery* **2015**, *14*, 561.
[5] D. Fukumura, J. Kloepper, Z. Amoozgar, D. G. Duda, R. K. Jain, *Nat. Rev. Clin. Oncol.* **2018**, *15*, 325.
[6] T. D. Wu, S. Madireddi, P. E. de Almeida, R. Banchereau, Y. J. Chen, A. S. Chitre, E. Y. Chiang, H. Iftikhar, W. E. O'Gorman, A. Au-Yeung, C. Takahashi, L. D. Goldstein, C. Poon, S. Keerthivasan, D. E. de Almeida Nagata, X. Du, H. M. Lee, K. L. Banta, S. Mariathasan, M. Das Thakur, M. A. Huseni, M. Ballinger, I. Estay, P. Caplazi, Z. Modrusan, L. Delamarre, I. Mellman, R. Bourgon, J. L. Grogan, *Nature* **2020**, *579*, 274.
[7] M. F. Fransen, M. Schoonderwoerd, P. Knopf, M. G. M. Camps, L. J. A. C. Hawinkels, M. Kneilling, T. Van Hall, F. Ossendorp, *JCI Insight* **2018**, *3*, 124507.
[8] M. H. Spitzer, Y. Carmi, N. E. Reticker-Flynn, S. S. Kwek, D. Madhireddy, M. M. Martins, P. F. Gherardini, T. R. Prestwood, J. Chabon, S. C. Bendall, L. Fong, G. P. Nolan, E. G. Engleman, *Cell* **2017**, *168*, 487.
[9] G. Bogle, P. R. Dunbar, *Immunol. Cell Biol.* **2010**, *88*, 172.
[10] D. Jones, E. R. Pereira, T. P. Padera, *Front. Oncol.* **2018**, *8*, 36.
[11] K. Murphy, C. Weaver, *Janeway's Immunobiology*, 9th ed., Garland Science, New York **2016**.
[12] A. S. Perelson, F. W. Wiegel, *J. Theor. Biol.* **2009**, *257*, 9.
[13] G. Lythe, R. E. Callard, R. L. Hoare, C. Molina-París, *J. Theor. Biol.* **2016**, *389*, 214.
[14] V. I. Zarnitsyna, B. D. Evavold, L. N. Schoettle, J. N. Blattman, R. Antia, *Front. Immunol.* **2013**, *4*, 485.
[15] M. K. Jenkins, J. J. Moon, *J. Immunol.* **2012**, *188*, 4135.
[16] U. H. von Andrian, C. R. Mackay, *N. Engl. J. Med.* **2000**, *343*, 1020.
[17] A. A. Davis, V. G. Patel, *J. Immunother Cancer* **2019**, *7*, 278.
[18] T. Powles, L. Morrison, *Nat. Rev. Urol.* **2018**, *15*, 585.
[19] K. Aslan, V. Turco, J. Blobner, J. K. Sonner, A. R. Liuzzi, N. G. Nunez, D. de Feo, P. Kickingereder, M. Fischer, E. Green, A. Sadik, M. Friedrich, K. Sanghvi, M. Kilian, F. Cichon, L. Wolf, K. Jahne, A. von Landenberg, L. Bunse, F. Sahm, D. Schrimpf, J. Meyer, A. Alexander, G. Brugnara, R. Roth, K. Pfleiderer, B. Niesler, A. von Deimling, C. Opitz, M. O. Breckwoldt, et al., *Nat. Commun.* **2020**, *11*, 931.
[20] I. X. Chen, K. Newcomer, K. E. Pauken, V. R. Juneja, K. Naxerova, M. W. Wu, M. Pinter, D. R. Sen, M. Singer, A. H. Sharpe, R. K. Jain, *Proc. Natl. Acad. Sci. USA* **2020**, *117*, 23684.
[21] D. S. Park, M. Robertson-Tessi, K. A. Luddy, P. K. Maini, M. B. Bonsall, R. A. Gatenby, A. R. A. Anderson, *Cancer Res.* **2019**, *79*, 5302.
[22] K.-A. Norton, C. Gong, S. Jamalian, A. Popel, *Processes* **2019**, *7*, 37.
[23] K. N. Margaris, R. A. Black, *J. R. Soc. Interface* **2012**, *9*, 601.
[24] G. E. Mahlbacher, K. C. Reihmer, H. B. Frieboes, *J. Theor. Biol.* **2019**, *469*, 47.
[25] J. D. Butner, D. Fuentes, B. Ozpolat, G. A. Calin, X. Zhou, J. Lowengrub, V. Cristini, Z. Wang, *IEEE Trans. Biomed. Eng.* **2020**, *67*, 1450.
[26] N. S. Adrar, K. Madani, S. Adrar, *PharmaNutrition* **2019**, *7*, 100142.
[27] M. R. Nikmaneshi, R. K. Jain, L. L. Munn, *PLoS Comput. Biol.* **2023**, *19*, e1011131.
[28] M. R. Nikmaneshi, B. Firoozabadi, *Biomech. Model. Mechanobiol* **2022**, *21*, 1233.
[29] M. R. Nikmaneshi, B. Firoozabadi, A. Mozafari, *Biotechnol. Bioeng.* **2021**, *118*, 3871.
[30] M. R. Nikmaneshi, B. Firoozabadi, A. Mozafari, L. L. Munn, *Sci. Rep.* **2020**, *10*, 3025.
[31] C. K. Buhler, R. S. Terry, K. G. Link, F. R. Adler, *Math. Biosci. Eng.* **2021**, *18*, 6305.
[32] M. Jafarnejad, C. Gong, E. Gabrielson, I. H. Bartelink, P. Vicini, B. Wang, R. Narwal, L. Roskos, A. S. Popel, *AAPS J.* **2019**, *21*, 79.
[33] H. Wang, O. Milberg, I. H. Bartelink, P. Vicini, B. Wang, R. Narwal, L. Roskos, C. A. Santa-Maria, A. S. Popel, *R. Soc. Open Sci.* **2019**, *6*, 190366..
[34] O. Milberg, C. Gong, M. Jafarnejad, I. H. Bartelink, B. Wang, P. Vicini, R. Narwal, L. Roskos, A. S. Popel, *Sci. Rep.* **2019**, *9*, 11286.
[35] S. Jamalian, C. D. Bertram, W. J. Richardson, J. E. Moore, *Am. J. Physiol. - Heart C* **2013**, *305*, H1709.
[36] S. Jamalian, M. J. Davis, D. C. Zawieja, J. E. Moore, *PLoS One* **2016**, *11*, e0148384.
[37] J. E. Moore, C. D. Bertram, *Annu. Rev. Fluid Mech.* **2018**, *50*, 459.
[38] C. D. Bertram, C. Macaskill, J. E. Moore, Jr., *J. Biomech. Eng.* **2019**, *141*, 111006.
[39] C. Kunert, J. W. Baish, S. Liao, T. P. Padera, L. L. Munn, *Proc. Natl. Acad. Sci. USA* **2015**, *112*, 10938.
[40] J. W. Baish, C. Kunert, T. P. Padera, L. L. Munn, *PLoS Comput. Biol.* **2016**, *12*, e1005231.
[41] K. E. Yost, A. T. Satpathy, D. K. Wells, Y. Qi, C. Wang, R. Kageyama, K. L. Mcnamara, J. M. Granja, K. Y. Sarin, R. A. Brown, R. K. Gupta, C. Curtis, S. L. Bucktrout, M. M. Davis, A. L. S. Chang, H. Y. Chang, *Nat. Med.* **2019**, *25*, 1251.
[42] M. R. Nikmaneshi, R. K. Jain, L. L. Munn, *PLoS Comput. Biol.* **2023**, *19*, e1011131.
[43] M. G. Harisinghani, A. O'Shea, *Atlas of lymph node anatomy*, Springer, Berlin **2013**.
[44] V. V. Ganusov, J. Auerbach, *PLoS Comput. Biol.* **2014**, *10*, e1003586.
[45] B. Breart, P. Bousso, *Eur. J. Immunol.* **2016**, *46*, 2730.
[46] J. B. Hay, B. B. Hobbs, *J. Exp. Med.* **1977**, *145*, 31.
[47] Q. Wang, Y. Fang, C. Li, T. L. Leong, M. Provencio, I.-J. Oh, Z. Zhang, C. Su, *Transl. Lung Cancer Res.* **2023**, *12*, 312.
[48] O. Bylicki, P. Tomasini, G. Radj, F. Guisier, I. Monnet, C. Ricordel, L. Bigay-Game, M. Geier, C. Chouaid, C. Daniel, *Eur. J. Cancer* **2023**, *183*, 38.
[49] L. A. Huppert, A. I. Daud, *J. Clin. Oncol.* **2021**, *39*, 2637.
[50] O. Hamid, C. Robert, A. Daud, M. S. Carlino, T. C. Mitchell, P. Hersey, J. Schachter, G. V. Long, F. S. Hodi, J. D. Wolchok, A. Arance, J. J. Grob, A. M. Joshua, J. S. Weber, L. Mortier, E. Jensen, S. J. Diede, B. H. Moreno, A. Ribas, *Eur. J. Cancer* **2021**, *157*, 391.
[51] D. M. Lussier, E. Alspach, J. P. Ward, A. P. Miceli, D. Runci, J. M. White, C. Mpoy, C. D. Arthur, H. N. Kohlmiller, T. Jacks, M. N. Artyomov, B. E. Rogers, R. D. Schreiber, *Proc. Natl. Acad. Sci. USA* **2021**, *118*, e2102611118.
[52] H. Menon, D. Chen, R. Ramapriyan, V. Verma, H. B. Barsoumian, T. R. Cushman, A. I. Younes, M. A. Cortez, J. J. Erasmus, P. De Groot, B. W. Carter, D. S. Hong, I. C. Glitza, R. Ferrarotto, M. Altan, A. Diab, S. G. Chun, J. V. Heymach, C. Tang, Q. N. Nguyen, J. W. Welsh, *J. Immunother. Cancer* **2019**, *7*, 1.
[53] Z. S. Buchwald, T. H. Nasti, J. Lee, C. S. Eberhardt, A. Wieland, S. J. Im, D. Lawson, W. Curran, R. Ahmed, M. K. Khan, *J. Immunother. Cancer* **2020**, *8*, e000867.
[54] S. E. Henrickson, T. R. Mempel, I. B. Mazo, B. Liu, M. N. Artyomov, H. Zheng, A. Peixoto, M. P. Flynn, B. Senman, T. Junt, H. C. Wong, A. K. Chakraborty, U. H. Von Andrian, *Nat. Immunol.* **2008**, *9*, 282.
[55] K.-A. G. Buela, R. L. Hendricks, *J. Immunol.* **2015**, *194*, 379.
[56] K. E. Yost, H. Y. Chang, A. T. Satpathy, *Science* **2021**, *372*, 130.
[57] B. Neupert, N. Olimpo, K. Nguyen, D. Nguyen, M. Knitz, M. Hoen, *Nat. Commun.* **2022**, *13*, 7015.
[58] L. B. Darragh, J. Gadwa, T. T. Pham, B. Van Court, B. Neupert, N. A. Olimpo, K. Nguyen, D. Nguyen, M. W. Knitz, M. Hoen, S. Corbo, M. Joshi, Y. Zhuang, M. Amann, X. J. Wang, S. Dow, R. M. Kedl, V. Samedi, M. K. Boss, S. D. Karam, *Nat. Commun.* **2022**, *13*, 7015.
[59] J. T. Poleszczuk, K. A. Luddy, S. Prokopiou, M. Robertson-Tessi, E. G. Moros, M. Fishman, J. Y. Djeu, S. E. Finkelstein, H. Enderling, *Cancer Res.* **2016**, *76*, 1009.

ADVANCED SCIENCE
Open Access

Supporting Information

for *Adv. Sci.*, DOI 10.1002/advs.202304076

Transport Barriers Influence the Activation of Anti-Tumor Immunity: A Systems Biology Analysis

*Mohammad R. Nikmaneshi, James W. Baish, Hengbo Zhou, Timothy P. Padera and Lance L. Munn**

Supplemental Material

Analysis of systemic transport barriers for the activation of anti-tumor immunity

Mohammad R. Nikmaneshi[1], Timothy P. Padera[1], James W. Baish[2], and Lance Munn.[1,*]

[1] Department of Radiation Oncology, Massachusetts General Hospital and Harvard Medical School, Boston, MA 02114, USA

[2] Biomedical Engineering, Bucknell University, Lewisburg, PA 17837, USA

* munn@steele.mgh.harvard.edu

CONTENTS

Supplementary Data and Figures

Estimation of lymph node visitation probabilities

Only a small fraction of total blood flow goes through lymph nodes, and each time a naive T cell makes a pass through the blood circulation, it can take a different path. Because there is no apparent mechanism for directing a blood-borne cell to one organ rather than another, or to the lymph node circulation rather than other parallel arterial paths, we assume these to be random processes. Based on this, and considering known circulation times and volumes, we can make a rough estimation of the probability that a specific naive T cell visits a lymph node that contains antigen (Figure 1S). In this estimation, we assume the volume of a human is 66 L and the number of organs (lymphosomes) is 8 (as in the simulations). The average volume of all nodes in each lymph node region (complex of multiple LNs region, each region approximately 63 LNs) is 34.7 ml. With this, the fractional volume of a single LN cluster relative to the body volume is 5.26×10^{-4}. Therefore, the fractional volume of each LN is equal to $5.26\times10^{-4}/63 = 8.34\times10^{-6}$.

In humans, blood circulates approximately once per minute. However, immune cells do not circulate this quickly because of significant residence times in capillary beds and lymph nodes. We assume that in the case that the nT cells does not enter a lymph node, the average circulation time is approximately 3 min due to the resistance in capillary beds [1]. If the nT cell enters a lymph node, the residence time is much longer (~10 hr) [1]. According to our stochastic model, each nT cell finds a LN region ~1.33 time per day (see figure 2 of the main text). If the residence time of a nT cell in a LN is 10hr, then on average, each nT cell is sequestered in a lymph node for 1.33×10 hours each day. Therefore, the effective average time that a nT cell actively circulates each day can be approximated by (24 hr-13.33 hr) ×60 ~ 640 min. If we assume that the circulation time is 3 min through organs other than lymph nodes, then the cell can circulate (640/3)+1(for residency in LNs) ~ 214 times per day. Therefore, the probabilities that a nT cell visits any specific lymph node in a given day can be calculated by

$(1-(1-8.34\times10^{-6})^{214}) \times 100 = 0.18$ %.

We can extend this analysis to estimate the probability of a given nT cell visiting any positive node in a 24 hour period as a function of the number of positive nodes (Fig. S1).

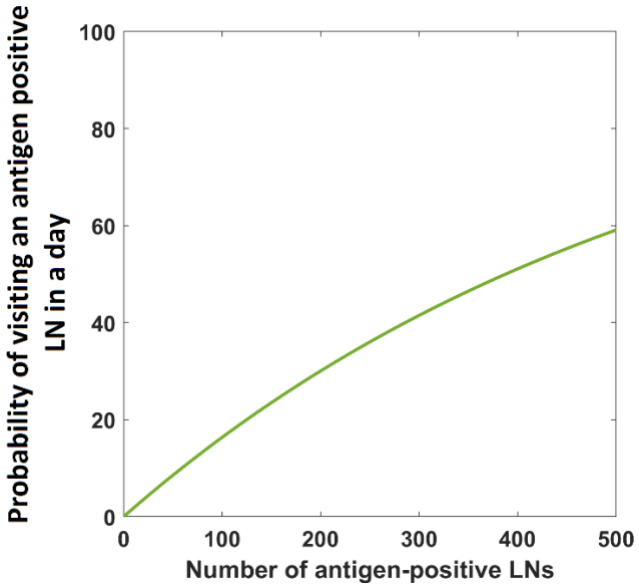

Figure. S1. Probability that a circulating n T cell visits an antigen-containing LN per day. Calculations are based on the relative blood flow through a lymph node in humans, estimated by tissue volumes. As more LNs receive antigen, the probability increases.

Determination of the time threshold for tumor elimination (for the definition of responders)

We assume that the tumor has been growing for some time before the T cells are activated and begin to attack the cancer cells. In our simulations, even if a nT cell gets activated, if the T cells accumulate in the tumor too

slowly, then the tumor can out-proliferate the effector T cells and survive. Thus, there is a critical size of tumor above which it is too late for nT cell activation to result in tumor eradication. To estimate this threshold time for activation of T cells, we performed multiple runs of a simplified model. The simplified model has four parameters for vascular tumor growth, avascular tumor growth, T cell proliferation, and T cell killing of tumor cells. The tumor growth parameters of the simplified model were determined by curve fitting of the tumor growth profile for the complete model. The T cell proliferation rate and tumor -T cell reaction parameters were set by curve fitting with the tumor restrained profile of our complete model for the responder case with minimum activation time. With these assumptions, we can find the activation time that results in stable tumor size -- that is, where the T cells keep the tumor size stable. Later activation allows the tumor to continue growing (designated "non-responder") while earlier activation results in tumor eradication (designated "responder"). The analysis concludes that the critical time for activation is 4.62 days; activation at this time results in a tumor size reduction (TSR) ratio equal to ~ 0.7 at the 2 week time point (Fig. S2).

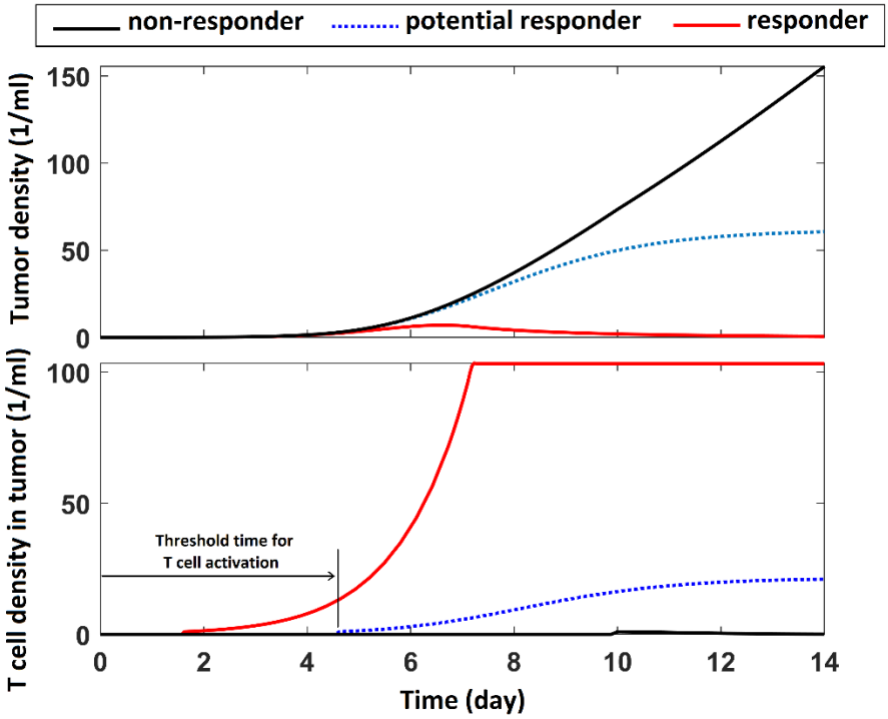

Figure. S2. Estimation of critical time for T cell activation to eliminate the tumor. The critical time is 4.62 days.

Impact of LN-FFR on radiotherapy responses:

To investigate the effect of LN-FFR on immune activation and radiation performance compared to the results of Figure 6 of the main text (where LN-FFR was fixed at 10%), we repeated the simulations with LN-FFR values of 5%, 1%, and 0.5%. The results of T cell accumulation in the TDLN and tumor growth for low and high antigen patients with LN-FFR equal to 5%, 1%, and 0.5% are shown in Figs. S3, S4 and S5, respectively.

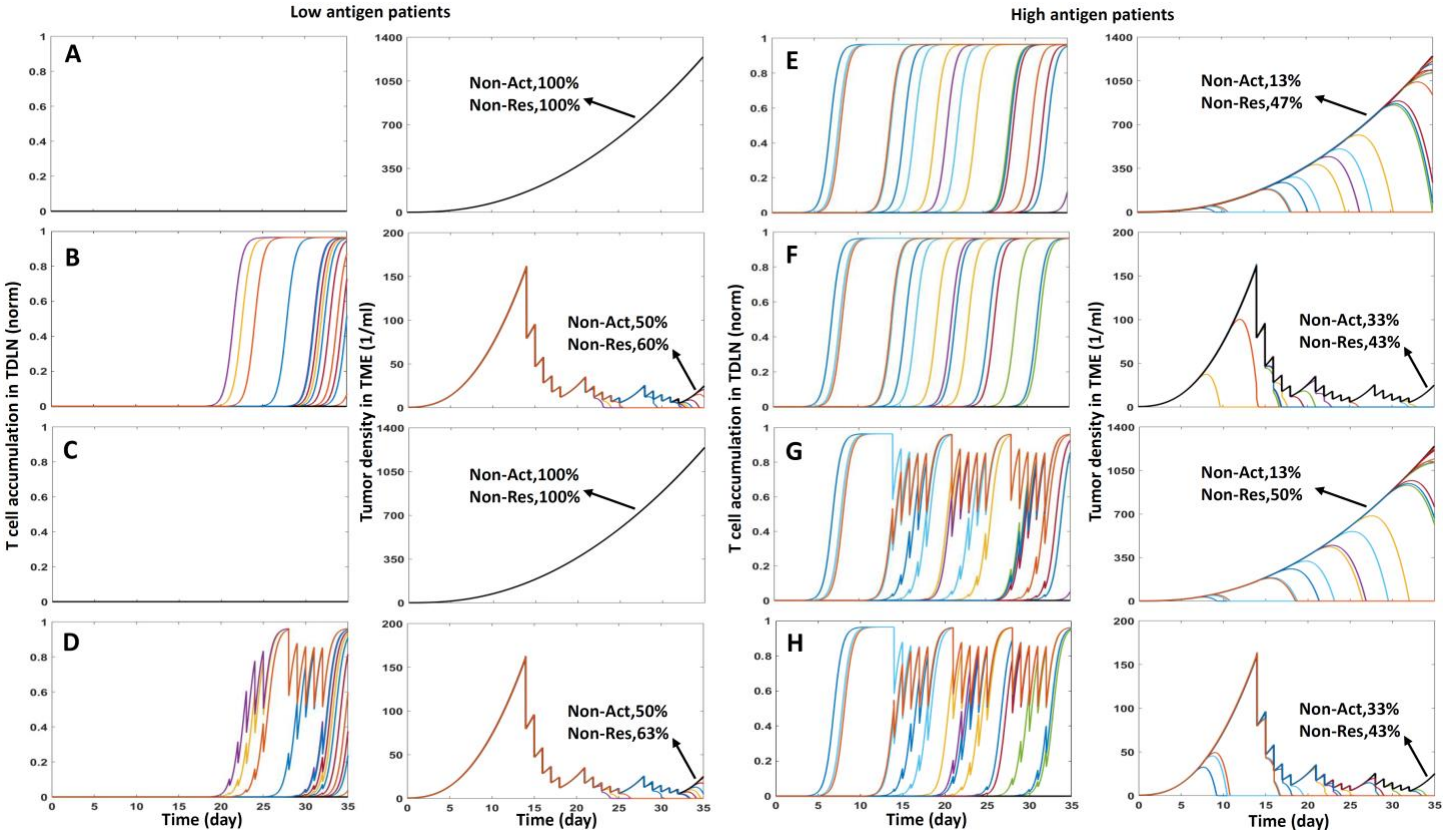

Figure S3. Effect of radiotherapy on tumor-immune response in low and high antigen patients with LN-FFR equal to 5%. 30 cases were simulated for each condition. RT starts on day 14, with daily dose of 2 Gy, except two days of weekend, administered over three weeks. A) Non-irradiated low antigen patients, B) RT on tumor of low antigen patients, C) radiation applied to the TDLN of low antigen patients, D) RT on tumor and TDLN of low antigen patients, E) non-irradiated high antigen patients, F) RT on tumor of high antigen patients, G) RT on TDLN of high antigen patients, H) RT on tumor and TDLN of high antigen patient. Black line shows patients in which T-cell activation does not occur. Colored lines show the T cell accumulation and tumor size in individual patients who have T-cell activation.

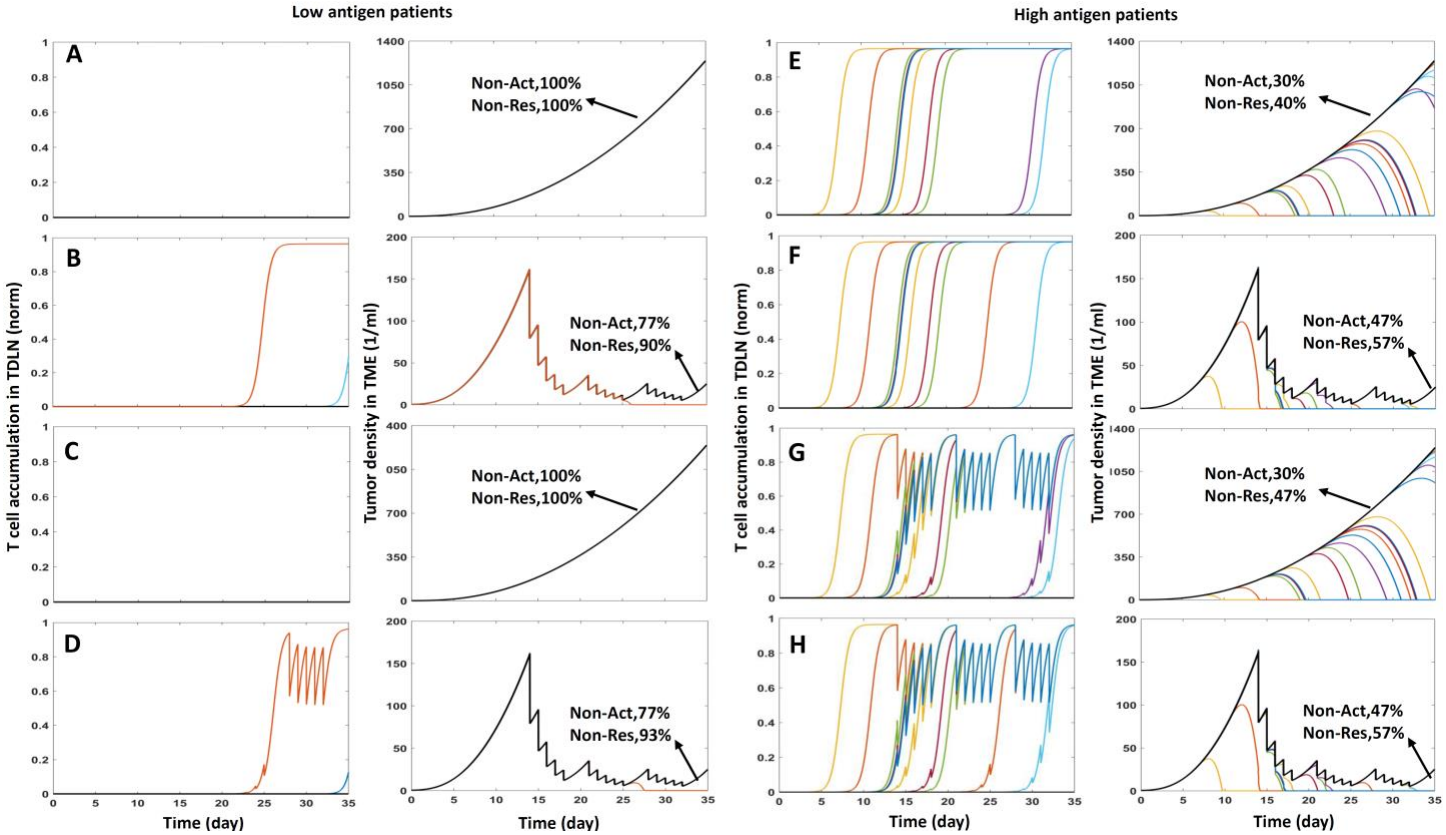

Figure S4. Effect of radiotherapy on tumor-immune response in low and high antigen patients with LN-FFR equal to 1%. 30 cases were simulated for each condition. RT starts on day 14, with daily dose of 2 Gy, except two days of weekend, administered over three weeks. A) Non-irradiated low antigen patients, B) RT on tumor of low antigen patients, C) radiation applied to the TDLN of low antigen patients, D) RT on tumor and TDLN of low antigen patients, E) non-irradiated high antigen patients, F) RT on tumor of high antigen patients, G) RT on TDLN of high antigen patients, H) RT on tumor and TDLN of high antigen patient. The black line shows patients in which T-cell activation does not occur. The colored lines show the TDLN T cell accumulation and tumor size in individual patients who have T-cell activation. Tumor size and T cell numbers are stochastically increased by activation, and are decreased by radiation treatment.

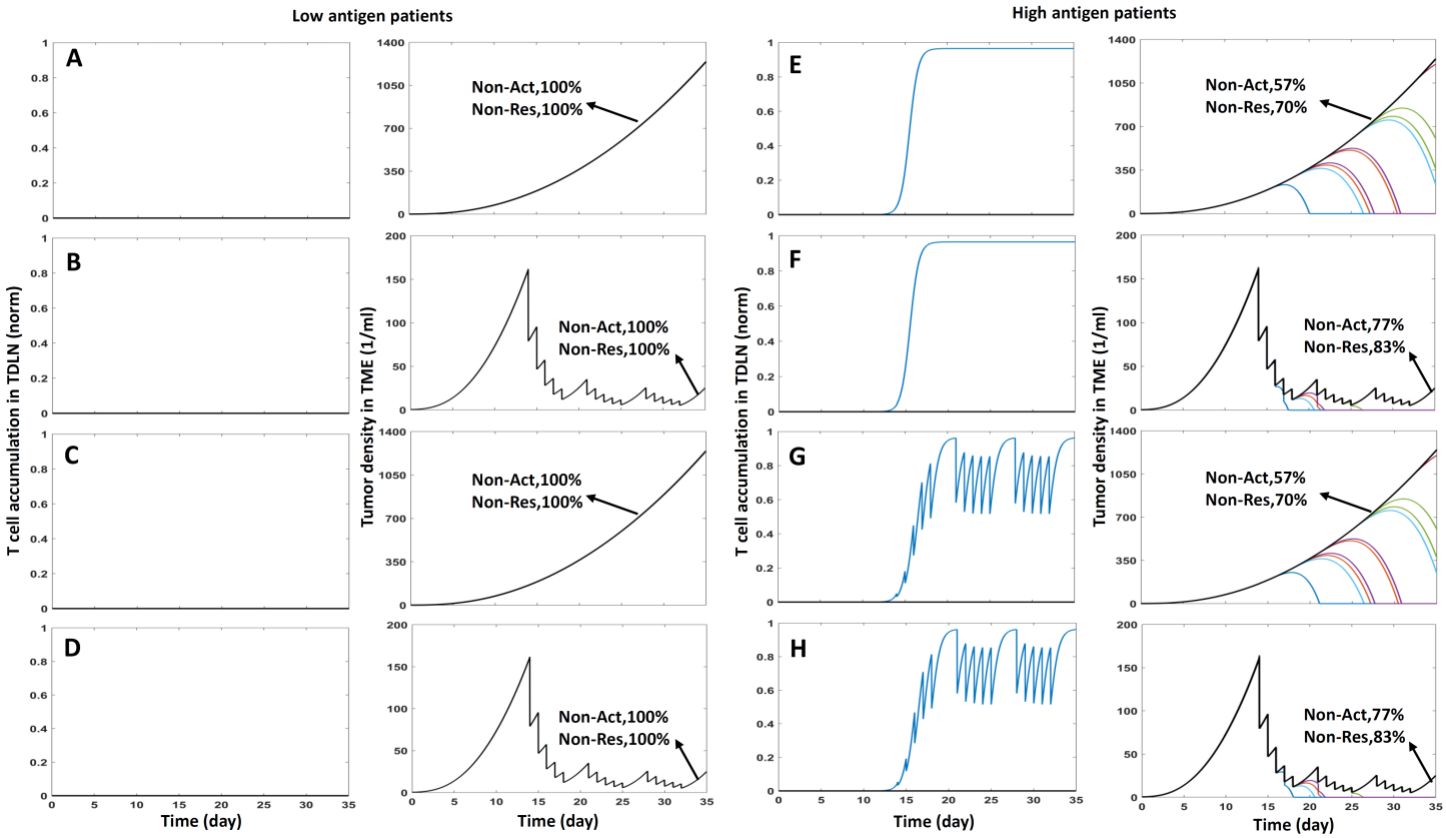

Figure S5. Effect of radiotherapy on tumor-immune response in low and high antigen patients with LN-FFR equal to 0.5%. 30 cases were simulated for each condition. RT starts on day 14, with daily dose of 2 Gy, except two days of weekend, administered over three weeks. A) Non-irradiated low antigen patients, B) RT on tumor of low antigen patients, C) radiation applied to the TDLN of low antigen patients, D) RT on tumor and TDLN of low antigen patients, E) non-irradiated high antigen patients, F) RT on tumor of high antigen patients, G) RT on TDLN of high antigen patients, H) RT on tumor and TDLN of high antigen patient. The black line shows patients in which T-cell activation does not occur. The colored lines show the TDLN T-cell accumulation and tumor size in individual patients who have T-cell activation. Tumor size and T cell numbers are stochastically increased by activation, and are decreased by radiation treatment.

Consistent with the results with 10% LN-FFR (Figure 6 of the main text), for high antigen patients, RT applied to the tumor decreases activation. RT applied to the TDLN affects tumor shrinkage (and calculated response rates) because of the damage to proliferating effector T cells in the node. Applying RT to both the tumor and TDLN combines these effects. For low antigen patients, radiation enhances activation, except in the 0.5% LN-FFR case, whether it is applied to the tumor or tumor and TDLN (see panels A-D of Figs. S3-S5). Decreasing the LN-FFR for high antigen patients consistently results in less activation and poorer response rates because the decreased LN-FFR delays activation in many patients. Similar to the results shown in Figure 6 of the main text, RT applied to the TDLN decreases response rates and has no effect on T cell activation. For low antigen patients with LN-FFR equal to 1% (Figure S4), RT applied to the tumor can cause activation for a few patients (Fig. S4, B and D). However, decreasing LN-FFR to 0.5% (Figure S5) results in no benefit for low antigen patients in terms of activation when RT is applied to the tumor. For high antigen patients, RT applied to the tumor delays T-cell activation (because less antigen source is available) and consequently decreases response rate. **Note that by decreasing LN-FFR there are some differences in the accumulation plots for T cell accumulation in the TDLN and the corresponding tumor growth curves (i.e., tumor shrinkage when there is no T cell activation in the TDLN). In these cases, T cell activation occurs in a non-tumor draining lymph node. For instance, the minimum LN-FFR, 0.5%, in Fig.S5 results in the most activation in other LNs such as lung LNs instead of TDLN (Fig. S5 E-H).**

Comparison between immune checkpoint blockade (ICB), radiation and their combination:

We also compared RT, ICB and their combination for the patients with high antigen production and activated immune responses. Inhibition of T-cell killing results in only radiation-induced shrinking of the tumor (no ICB, Figure S6 A). Without radiation, but with T-cell killing, stochastic T-cell activation drives tumor shrinkage in some patients (Figure S6 B). Combining these effects result in additive tumor shrinkage, on a per-patient basis (Figure S6 C).

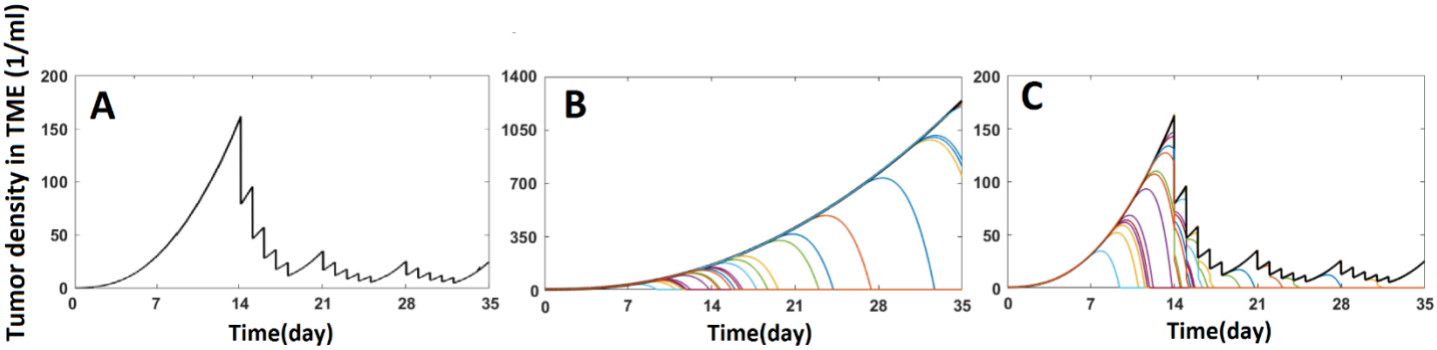

Figure S6. Comparison of RT, ICB and their combination therapy for high antigen patients with LN-FFR equal to 10%. A) RT applied to the tumor without the effect of ICB, so that activated T cells are unable to kill cancer cells. B) ICB is applied, allowing activated T cells to kill cancer cells. C) combination of ICB and RT applied to the tumor.

Removal of the TDLN delays immune activation:

Reports in the literature have shown that the tumor draining lymph node (TDLN) is important for the initiation of tumor immunity, as it is a primary location of antigen accumulation [2]. To investigate this, we simulated removal of the TDLN and monitored activation rates. When the TDLN is removed, we assume that antigen can travel systemically via the thoracic duct and blood circulation to accumulate in other LNs. We further assume that blood-borne antigen partitions into LNs according to the LN-FFR. We simulated 100 cancer patients for conditions of high antigen production rate and an LN-FFR of 10% and plotted the time required for T cell activation (Fig. S7-A).

In these simulations, there was activation in the LNs associated with the lung and gastrointestinal tissues. We did not observe activation in other lymph nodes because of systemic dilution and low accumulation rates of antigen in other tissues. Antigen accumulated in the abdominal LN more quickly than the lung LN due to the higher flow volume of lymph to the central LNs, so the antigen concentration surpasses the threshold earlier in that LN (red and purple dashed lines, Fig. S7-A). The activation time for each patient is shown by the red and purple circles. Note that in the 40 day period, 72/100 patients had activation, while 28/100 did not. 62 patients had activation occur in the lung, while 9 had activation in the abdominal LN. Interestingly, t_a is smaller for the abdominal LN (the antigen surpasses the threshold sooner), but t_t is smaller in the lung (activation is more efficient in the lung, after antigen is present). This is because of the higher blood flow into the lungs vs. the GI tissue. This allows the nT cell to sample the lung LN more often than the GI LN.

The cases of early T cell activation in the abdominal LN resulted in larger tumor size reductions compared with activations in the lung LN (Fig. S7-B). Therefore, resecting the TDLN delays T cell activation, and consequently, leads to a significant delay in tumor killing by the T cells. Comparison between Fig. S7-B and Fig. 5 of the main text for high antigen patients with LN-FFR 10% shows that resecting the TDLN increases the initiation time of the response from one week to five weeks. Therefore, compared to patients with an intact, functional TDLN, a delay around four weeks is conceivable for administrating ICB treatment for patients without TDLN.

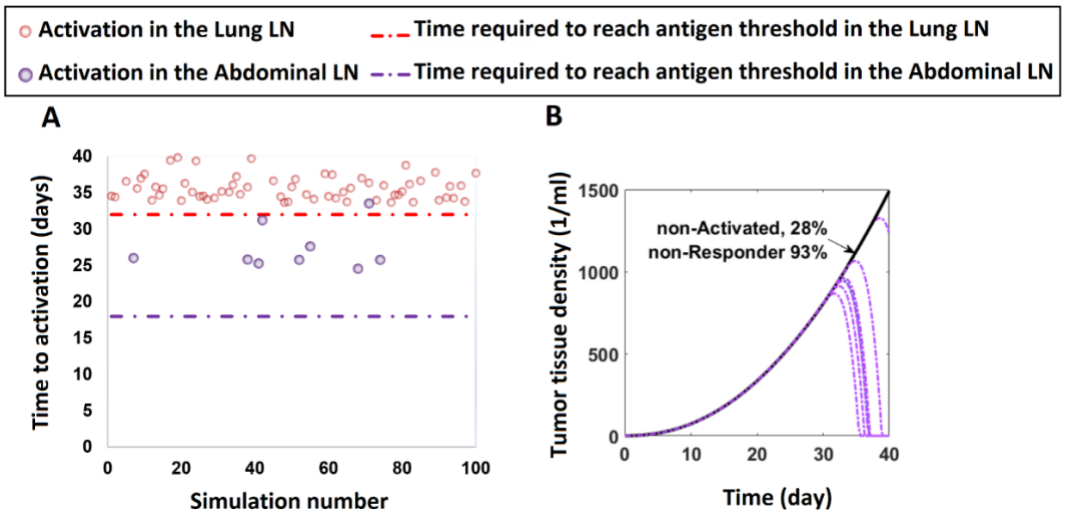

Figure S7. Removal of the TDLN affects T cell activation and tumor size reduction. A) After mathematical removal of the TDLN, we ran 100 simulations and recorded the time and location of nT cell activation. Activation time is indicated in pink for the lung LN and in violet for the central LN. B) Tumor size profiles of patients with TDLN resection over 40 days.

Model Parameter definitions:

In this model, each organ includes a tissue subcompartment and a LN subcompartment indexed with *i* and *LNi*, respectively. T^b and A^b are free T cell and antigen concentrations in blood stream, T^c captured T cell concentration on blood vessel inner surface, T^{ins} and A^{ins} are interstitial T cell and antigen concentrations, T^a and A^a are T cell and antigen concentrations in the arterial flow of heart, T^v and A^v are T cell and antigen concentrations in the venous flow of heart, *a* and *b* attachment and detachment rates of free T cells, J_t and J_a are respectively the transmigration rate of captured T cells passing through blood vessel wall and the perfusion rate of antigen across the vessel wall, ε is natural decay of antigen in interstitium.

In terms of fluid dynamics parameters, *Q* and *L* are blood flow rate and lymphatic flow rate, V^b and V^{ins} are the averaged volumes of blood vessels and interstitium, fi_t and fi_a are fractions of interstitial T cells and antigen that are drained by lymphatic vessels, respectively, which get into the local lymphatic flow. *f* and (1-*f*) are the fractions of blood flow rate to respectively supply the tissue part and lymph node part of each organ, *ff* is a fraction of lymphatic flow of each organ that is directly released into the systematic lymphatic flow; the remainder (1-*ff*) is the fraction of lymphatic flow from each organ that is released into the associated lymph node (Fig. 1).

For antigen-induced T cell proliferation, *S* is tumor-induced antigen function, *P* is antigen-induced T cell proliferation function, ρ proliferation rate of T cells in LN, A^{th} is the minimum antigen concentration to cause T cells proliferation, T^{th1} is the minimum concentration of T cells in LN to start local proliferation, T^{th2} is the maximum concentration of T cells that can be placed into each LN's paracortex, and when reached instantly stops T cell proliferation. a_c, $a_{c,I}$ and $a_{c,RT}$ are the antigen production rates of alive cancer cells, immune-induced apoptotic cancer cells, and apoptotic tumor cells by radiation.

In terms of anti-cancer immunity, k_1, k_{-1}, *and* k_2 are respectively the rates of tumor-T cell complex formation, tumor-T cell complex degradation, PD-L1/PD-1-based tumor cell killing, and PD-L1-induced T cell exhaustion, $\alpha_{T,C}$ the concentration of tumor-T cell complex, C_a the concentration of live tumor cells, $T^{exh}{}_{tumor}$ concentration of PD-L1$^+$(Treg)-induced exhausted T cell in tumor tissue, $C_{ap,I}$ and $C_{ap,RT}$ are the concentrations of PD-L1/PD-1-based and radiation-induced apoptotic cancer cells.

For the radiotherapy part of model, *SF* is the survival fraction of irradiated cells, ξ is scale factor for the radiosensitivity of cells, α and β are cell type-specific radiosensitivity parameters for cells, and D is dose of radiation. ξ, α and β are cell type-specific parameters.

For the tumor growth model, g_v and g_{av} are constant maximum rates of vascular and avascular tumor growth, λ_{a0} is M-M constant of avascular tumor growth, β_{ag} and ω_{ag} are, respectively, the maximum rate of angiogenesis and the maximum rate of vessel disruption, α_{vegf0} and θ_{vegf0} are the M-M constant for VEGF-induced angiogenesis and vessel disruption.

Detailed description of the model

I: Circulation and stochastic activation of naive T cells (nT cells)

First, we keep track of nT cell circulation, and their entry into various lymph nodes (Fig. S8). This is calculated based on relative blood flow rates into various organs and lymph nodes, with residence times assumed as in Table 1S. If an nT cell visits a lymph node where antigen concentration is above the threshold value, it transforms into an activated (effector) T cell, and we transition to the model in the next section.

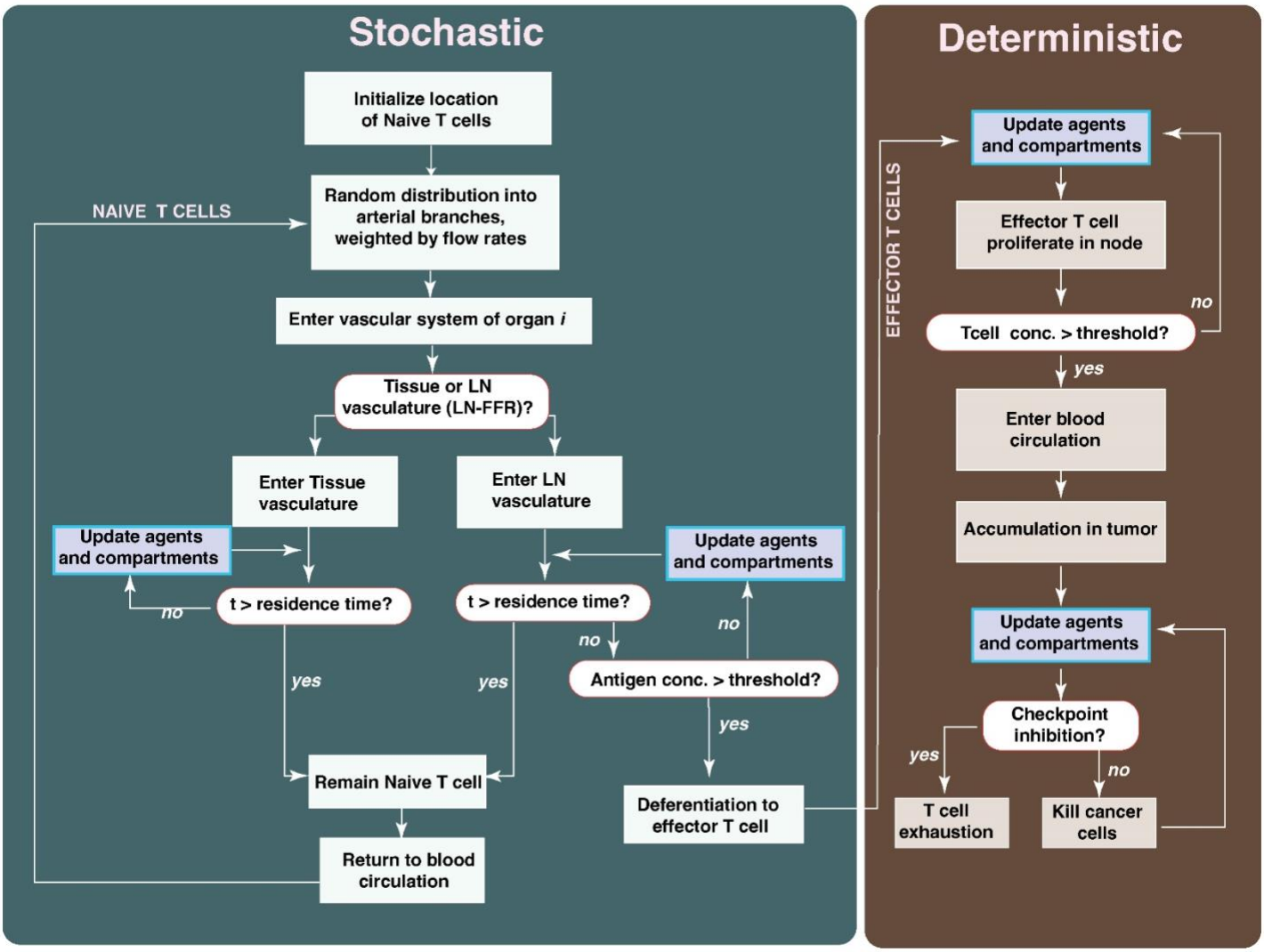

Figure S8. computational Flow chart for the model. The left hand side contains the stochastic algorithm for circulation and activation of naive T cells. The right hand side calculates the proliferation of activated T cells, their accumulation in the tumor and tumor killing. Note that for the presented simulations, the rate constant for checkpoint inhibition was set to 0.99, so there is nearly complete immune checkpoint inhibition and little T cell exhaustion. For the blue boxes "Update agents and compartments", we recalculate the tumor size, concentrations of antigen, T cells, angiogenic growth factors, tumor vasculature and flow rates in all compartments.

II: Proliferation and circulation of activated T cells (effector T cells); Tumor killing

The rest of the model description for effector T cell distribution applies after a naive T cell finds an antigen-rich lymph node and becomes activated. After activation, we define three different states of the T cells: 1) free T cells circulating in the blood stream, 2) T cells attached to the blood vessel endothelium, and 3) T cells transmigrated into the tumor interstitium.

Tumor compartment

In the compartmental model, the tumor can be hosted by any of the organs. Here we simulate a tumor growing in the breast.

a) T-cell trafficking through the blood circulation and tumor tissue:

The mass balance for T cells in the tumor bloodstream (T^b_{tumor}) is:

$$\frac{dT^b_{tumor}}{dt} = \begin{pmatrix} f_{tumor}\, Q_{tumor}\, T^b_{Heart} - (\, f_{tumor} Q_{tumor} - L_{tumor})\, T^b_{tumor} \\ - a_{tumor}\, T^b_{tumor}\, V^b_{tumor} \\ + d_{tumor}\, T^c_{tumor}\, V^b_{tumor} \end{pmatrix} / V^b_{tumor} \qquad (1a)$$

where the first term is the flow of T cells from the arterial blood into the tumor; the second term is the flow of T cells out of the tumor via the venous blood flow that equals inlet arterial flow minus filtered interstitial flow/lymphatic flow ($f\,Q$ - L); the third term represents the binding of T cells to the tumor endothelium, and the last term is the detachment of cells from the endothelium. In the tumor compartment, we assume that the vascular attachment and detachment rates (a and d) of T cells depends on tumor size (Table. S).

The mass balance for the T cells attached to the vessel wall (T^c_{tumor}) is:

$$\frac{dT^c_{tumor}}{dt} = \left(\, a_{tumor}\, T^b_{tumor}\, V^b_{tumor} - d_{tumor}\, T^c_{tumor}\, V^b_{tumor} - J_{t,tumor}\, T^c_{tumor}\, V^b_{tumor} \,\right) / V^b_{tumor} \qquad (1b)$$

Where the first term is the binding of T cells to the vessel wall, the second term is the detachment and the third term is transmigration.

The mass balance for T cells in the tumor tissue (T^{ins}_{tumor}) is:

$$\frac{dT^{ins}_{tumor}}{dt} = \begin{pmatrix} J_{t,tumor}\, T^c_{tumor}\, V^b_{tumor} - L_{tumor}\, T^{ins}_{tumor}\, fi_{t,tumor} \\ -\left(k_1 (1 + \beta_v \frac{v}{v + \alpha_v})\, T^{ins}_{tumor}\, C_a - (k_{-1} + k_2 \;\; p_r)\alpha_{T,C} \right) V^{ins}_{tumor} \end{pmatrix} / V^{ins}_{tumor} \qquad (1c)$$

Where the first term is T cell transmigration into the tumor from blood vessels, the second term is T cell entry into lymphatic vessels; the third term represents the binding of T cells to cancer cells and the last term is de-conjugation of T cells from cancer cells, which can occur immediately after generation of tumor/T cell complex ($\alpha_{T,C}$) at a constant rate; k_{-1}, or after killing cancer cells by effector T cells (with the reaction rate equals $k_2 \;\; p_r$).

We assume that effector T cells don't leave tumor interstitium, thus the drainage fraction of T cells in tumor tissue ($fi_{t,tumor}$) in the second term is set by zero (Table. S). Since the tumor tissue restricts T cell penetration into deep regions of tumor, we assume that angiogenic vessels can help T cells penetrate tumor tissue to increase the formation probability of cancer/T cell complex. Note that in these simulations, effector T cells are activated in lymph nodes and delivered to tissues via the blood stream and assumed to enter the tumor according to equation 1b. Therefore, we do not consider explicitly the effects of chemokines that might affect their migration once they arrive at the target site.

We assume that T cells become exhausted at a constant rate. The mass balance for exhausted T cells (T^{exh}_{tumor}) is:

$$\frac{dT_{tumor}^{exh}}{dt} = \left(k_2 \ (1-p_r)\ \alpha_{T,C} \right) \tag{1d}$$

Where $k_2\ (1-p_r)$ is the rate of T cell exhaustion due to immune checkpoint (IC) mechanism of cancer cells. Note that for the present analysis, we assume that pr is ~1, so this mechanism is not significant.

b) Tumor cell proliferation, angiogenesis and death:

Tumor growth and angiogenesis: cancer cells proliferate, are bound by T cells and can de-conjugate and return to the active cell population.

The mass balance for active cancer cells, C_a is:

$$\frac{dC_a}{dt} = \begin{pmatrix} g_v \left(\frac{v}{C_a + v}\right) C_a + g_{av} \left(\frac{C_a}{C_a + \lambda_{a0}}\right) + (k_{-1} + k_2 \ (1-p_r))\alpha_{T,C} \\ -k_1 \left(1 + \beta_v \frac{v}{v + \alpha_v}\right) T_{tumor}^{ins} \ C_a \end{pmatrix} \tag{2a}$$

Where the first term is the vascularized tumor growth as a function of angiogenic vessels,*v*, and active cancer cells, C_a, the second term is avascularized tumor growth in the form of Michaelis–Menten model, the third term is the sumation of the de-conjugation rate of cancer cells from tumor/T cell complexes ($k_{-1}\,\alpha_{T,C}$) and the IC rate of cancer cells ($k_2\,(1-p_r)\,\alpha_{T,C}$) (which is neglible here, since pr is ~0). The last term is the generation of tumor/T cell complexes with the help of angiogenic vessels.

The mass balance for cancer-immune cell conjugates $\alpha_{T,C}$ is:

$$\frac{d\,\alpha_{T,C}}{dt} = \left(k_1 \left(1 + \beta_v \frac{v}{v + \alpha_v}\right) T_{tumor}^{ins} \ C_a - \left(k_{-1} + k_2\right) \alpha_{T,C} \right) \tag{2b}$$

Where the first term is production rate of complex formation as a function of angiogenic vessels that can help T cells penetrate deeper regions of cancer and make complex with inner cells, and the second term is reduction rate of cancer/T cell complex immediately after formation with reversibility rate (k_{-1}) and after doing reaction with T cells with rate k_2.

To model angiogenesis, we assumed that cancer cells secrete vascular endothelial growth factors (VEGF) that can stimulate endothelial cells to start angiogenesis. The concentration of tumor-induced VEGF, c_{vegf}, is given by:

$$\frac{dc_{vegf}}{dt} = \left(\eta_{ag} \ (C_a + \alpha_{T,C}) - \varepsilon_{vegf} \ c_{vegf} \right) \tag{2c}$$

where the first term is the production rate of VEGF by cancer cells (both de-conjugated and conjugated with T cells), and the second term is the natural decay of VEGF.

To model angiogenesis mechanism for vascular density, we developed equation (2d) based on VEGF concentration. Tumor-induced angiogenesis changes the angiogenic vessel density, v, through Eq. 2d:

$$\frac{dv}{dt} = \beta_{ag} \left(\frac{c_{vegf}}{c_{vegf} + \alpha_{vegf\,0}} \right) - \omega_{ag} \left(1 - \frac{c_{vegf}}{c_{vegf} + \theta_{vegf\,0}} \right) v \tag{2d}$$

where the first term is the production of angiogenic vessels in response to VEGF and the second term is vascular pruning in response to low VEGF conditions.

Cancer cell death is induced by the immunogenic and non-immunogenic mechanisms. As the part of immunogenic mechanism of cancer cell death, the cancer cells are killed by effector T cells ($C_{ap,I}$) and the rate of this reaction is calculated by:

$$\frac{dC_{ap,I}}{dt} = \left(k_2 \;\; p_r \;\; \alpha_{T,C} \right) - \varepsilon_{ap,I} \;\; C_{ap,I} \tag{2e}$$

In this model, non-immunogenic mechanisms of cancer cell death are caused by radiotherapy. The linear-quadratic model as a key tool in radiation biology provides a simple relationship between cell survival and delivered dose (set of Eqs. 2f) and has been used extensively to analyze and predict responses to ionizing radiation both in vitro and in vivo. To include the effect of radiation on cancer cell death, the linear-quadratic model of radiation damage given in Eq. 2f is applied for each application of RT [3].

Where *SF* is the survival fraction of irradiated cells, ξ is scale factor for the radiosensitivity of cells, α and β are cell type-specific radiosensitivity parameters for cells, and D is dose of radiation.

$$C_a^{\overset{+}{t}} = C_a^{\overset{-}{t}} \; SF_c, \quad \alpha_{T,C}^{\overset{+}{t}} = \alpha_{T,C}^{\overset{-}{t}} \; SF_c \tag{2f}$$

$$C_{ap,RT}^{\overset{+}{t}} = C_{ap,RT}^{\overset{-}{t}} + (C_a^{\overset{-}{t}} + \alpha_{T,C}^{\overset{-}{t}}) \; (1 - SF_c)$$

$$SF_c = \exp(-\xi_c(\alpha_c \; D + \beta_c \; D^2))$$

The decay of RT-killed cancer cells is represented by,

$$\frac{dC_{ap,RT}}{dt} = -\varepsilon_{ap,RT} \;\; C_{ap,RT} \tag{2g}$$

c) Effect of radiation on non-cancerous cells:

The same mechanism can be applied for the vessels and T cells exposed to radiation therapy;

To determine the effect of radiation on angiogenic vessels, the linear-quadratic model of radiation is applied as Eq. 2h, after each application of RT,

$$v^{\overset{+}{t}} = v^{\overset{-}{t}} \; SF_v \tag{2h}$$

$$v_{ap,RT}^{\overset{+}{t}} = v_{ap,RT}^{\overset{-}{t}} + v^{\overset{-}{t}} \; (1 - SF_v)$$

$$SF_v = \exp(-\xi_v(\alpha_v \; D + \beta_v \; D^2))$$

The decay of RT-killed angiogenic vessel can be represented by,

$$\frac{dv_{ap,RT}}{dt} = -\varepsilon_{ap,RT} \;\; v_{ap,RT}, \tag{2i}$$

To determine the radiation effect on T cells the linear-quadratic model of radiation is applied as Eq. 2h, after each application of RT,

$$T^{+}_{tumor} = T^{-}_{tumor}\ SF_T \tag{2j}$$

$$T^{+}_{ap,RT} = T^{-}_{ap,RT} + T^{-}_{tumor}\ (1 - SF_T)$$

$$SF_T = \exp(-\xi_T(\alpha_T\ D + \beta_T\ D^2))$$

The decay of RT-killed T cells can be represented by,

$$\frac{dT_{ap,RT}}{dt} = -\varepsilon_{ap,RT}\ \ T_{ap,RT} \tag{2k}$$

d) Antigen distribution in the blood circulation and tumor interstitium:

Antigen is produced in the tumor and moves into the lymph and then the blood. The equation for antigen in the tumor blood supply (A^b_{tumor}) is:

$$\frac{dA^b_{tumor}}{dt} = \left(f_{tumor}\ Q_{tumor}\ A^b_{Heart} - \left(f_{tumor}\ Q_{tumor} - L_{tumor} \right) A^b_{tumor} - J_{a,tumor}\ A^b_{tumor}\ V^b_{tumor} \right) / V^b_{tumor} \tag{3a}$$

where the first term is the flow of antigen into the tumor via the bloodstream, the second term is antigen leaving the tumor via the blood and lymphatic systems and the last term is the filtration of antigen from the blood into the tumor tissue.

The source of antigen is live tumor cells and dying tumor cells (killed by radiation or T cells).

$$\frac{dA^{ins}_{tumor}}{dt} = \left(S\ V^{ins}_{tumor} + J_{a,tumor}\ A^b_{tumor}\ V^b_{tumor} - L_{tumor}\ A^{ins}_{tumor}\ \ fi_{a,tumor} - \varepsilon_{tumor}\ A^{ins}_{tumor}\ V^{ins}_{tumor} \right) / V^{ins}_{tumor} \tag{3b}$$

$$S = \ (a_c\ C_a + a_{cT}\ \alpha_{T,C} + a_{c,I}\ C_{ap,I} + a_{c,RT}\ C_{ap,RT})$$

e) T-cell trafficking to the tumor draining lymph node (TDLN)

T cells enter the TDLN via the blood stream; they can exit with the blood flow, and the naïve T cell can be captured; however, effector T cells cannot be captured by attaching to the HEVs in the node:

$$\frac{dT^b_{TDLN}}{dt} = \begin{pmatrix} (1 - f_{tumor})\ Q_{tumor}\ T^b_{tumor} \\ -\left((1 - f_{tumor})\ Q_{tumor} - L_{TDLN} \right) T^b_{TDLN} \end{pmatrix} / V^b_{TDLN} \tag{4a}$$

T cells enter from upstream tissue via lymph flow; they can also be killed by radiation treatments:

$$\frac{dT^{ins}_{TDLN}}{dt} = \begin{pmatrix} P(A^{ins}_{TDLN}, T^{ins}_{TDLN}) \\ +(1 - ff_{tumor})\ L_{tumor}\ T^{ins}_{tumor}\ \ fi_{t,tumor} \\ -\left((1 - ff_{tumor})\ L_{tumor} + L_{TDLN} \right) \\ \times (H(T^{th}_{TDLN} - T^{ins}_{TDLN})\ fi_{t,TDLN} + H(T^{ins}_{TDLN} - T^{th}_{TDLN}))T^{ins}_{TDLN} \end{pmatrix} / V^{ins}_{TDLN} \tag{4b}$$

$$P(A^{ins}_{TDLN}, T^{ins}_{TDLN}) = \rho_{TDLN}\ \ T^{ins}_{TDLN}\ \ V^{ins}_{TDLN}\ \ H_{(A^{ins}_{TDLN} - A^{th})}\ \ H_{(T^{ins}_{TDLN} + nTcell)}\ H_{(T^{th}_{TDLN} - T^{ins}_{TDLN})}$$

where the first term is the proliferation rate of T cells in antigen-positive LNs, the second term is T cell flow from lymphatic flow of tissue into LNs, and the last term is the fraction of T cells that bypasses the LN and exits at the efferent lymphatic vessel. The proliferation rate of T cells is a function of antigen concentration in the LN, nT cell presence in the LN, and the level of effector T cells in the LN.

f) Antigen distribution in TDLN

The mass balance for antigen in the blood circulation of the tumor draining lymph node (A^b_{TDLN}) is:

$$\frac{dA^b_{TDLN}}{dt} = \begin{pmatrix} (1-f_{tumor})\, Q_{tumor}\; A^b_{heart} \\ -\left((1-f_{tumor})\, Q_{tumor} - L_{TDLN}\right) A^b_{TDLN} \\ -J_{a,TDLN}\; A^b_{TDLN}\; V^b_{TDLN} \end{pmatrix} / V^b_{TDLN} \tag{5a}$$

where the first term is the flow of antigen from the tumor to the LN in the blood; the second term is the flow of antigen in the efferent blood stream, and the last term is the antigen that crosses the blood vessel to enter the LN.

The mass balance for antigen within the tumor draining lymph node tissue (A^{ins}_{TDLN}) is:

$$\frac{dA^{ins}_{TDLN}}{dt} = \begin{pmatrix} J_{a,TDLN}\; A^b_{TDLN}\; V^b_{TDLN} + (1-ff_{TDLN})\; L_{tumor}\; A^{ins}_{tumor}\; fi_{a,tumor} \\ -\left((1-ff_{TDLN})\, L_{tumor} + L_{TDLN}\right) A^{ins}_{TDLN}\; fi_{a,TDLN} \\ -\varepsilon_{TDLN}\; A^{ins}_{TDLN}\; V^{ins}_{TDLN} \end{pmatrix} / V^{ins}_{TDLN} \tag{5b}$$

where the first term is antigen entering the LN from the blood supply; the second term is the flow of antigen with the lymph via the afferent lymphatic vessel; the third term represents the fraction of antigen that bypasses the LN and exits at the efferent lymphatic vessel. The last term is the degradation of antigen in the node.

Lung

a) T-cell trafficking in the blood and interstitial compartments

In other organs, such as lung, T cells enter and leave via the bloodstream; they also attach and detach from the vessel wall:

$$\frac{dT^b_{lung}}{dt} = \begin{pmatrix} Q_{lung}\; T^v_{Heart} - (Q_{lung} - L_{lung})\, T^b_{lung} \\ -a_{lung}\; T^b_{lung}\; V^b_{lung} \\ +d_{lung}\; T^c_{lung}\; V^b_{lung} \end{pmatrix} / V^b_{lung} \tag{6a}$$

The first term is the flow of T cells from the venous flow into the lung, the second term is the T cells leaving the lung via outlet of blood flow, the last terms are attachment and detachment rates of antigen from and to lung vessels.

T cells can extravasate into the interstitial compartment:

$$\frac{dT^c_{lung}}{dt} = \left(a_{lung}\; T^b_{lung}\; V^b_{lung} - d_{lung}\; T^c_{lung}\; V^b_{lung} - J_{t,lung}\; T^c_{lung}\; V^b_{lung} \right) / V^b_{lung} \tag{6b}$$

In this equation, the first term is the attachement rate of T cells to the lung vessels, the second term is the detachment rate of T cells from the lung vessels, and the last term is the transmigration rate of T cells from vessels to tissue.

T cells enter the lung tissue by transmigration, and leave via the lymphatic system:

$$\frac{dT_{lung}^{ins}}{dt} = \left(J_{t,lung}\ T_{lung}^{c}\ V_{lung}^{b} - L_{lung}\ T_{lung}^{ins}\ fi_{t,lung} \right) / V_{lung}^{ins} \tag{6c}$$

Where, the first term is the transmigration rate of T cells, and the second term is the T cell flow out of tissue part of lung.

b) Antigen distribution in blood and tissues

Blood-borne antigen can enter other tissues, including lung. The mass balance for antigen concentration in the blood compartment of the lung is:

$$\frac{dA_{lung}^{b}}{dt} = \left(Q_{lung}\ A_{Heart}^{v} - \left(Q_{lung} - L_{lung}\right) A_{lung}^{b} - J_{a,lung}\ A_{lung}^{b}\ V_{lung}^{b} \right) / V_{lung}^{b} \tag{7a}$$

where the first term is the flow of antigen from the venous flow into the lung, the second term is the flow of antigen out of the lung, and the last term is trasnmigration;

Antigen leaves the tissue via lymphatic drainage, and can also degrade:

$$\frac{dA_{lung}^{ins}}{dt} = \begin{pmatrix} J_{a,lung}\ A_{lung}^{b}\ V_{lung}^{b} - L_{lung}\ A_{lung}^{ins}\ fi_{a,lung} \\ -\varepsilon_{lung}\ A_{lung}^{ins}\ V_{lung}^{ins} \end{pmatrix} / V_{lung}^{ins} \tag{7b}$$

where the first term is the trasnmigration of antigen into lung tissue from blood vessels, the second term is antigen leaving the lung interstitium via the lymphatic system and the last term is the natural decay of antigen.

c) T-cell trafficking in the LN of the lung

T cells can enter/leave a LN via blood vessels; they attach and detach from HEVs:

$$\frac{dT_{LNlung}^{b}}{dt} = \begin{pmatrix} (1 - f_{lung})(Q_{lung} - L_{lung})T_{lung}^{b} \\ -\left((1 - f_{lung})(Q_{lung} - L_{lung}) - L_{LNlung}\right)T_{LNlung}^{b} \end{pmatrix} / V_{LNlung}^{b} \tag{8a}$$

Where the first term is T cell flow from the outlet blood flow of the lung to the lung LNs and the second term is T cell flow leaving the LNs of lung via blood and lymphatic system.

T cells enter the node via transmigration or lymph flow; they can activate or flow out via lymph:

$$\frac{dT_{LNlung}^{ins}}{dt} = \begin{pmatrix} P(A_{LNlung}^{ins}, T_{LNlung}^{ins}) \\ +(1 - ff_{lung})\ L_{lung}\ T_{lung}^{ins}\ fi_{t,lung} \\ -\left((1 - ff_{lung})\ L_{lung} + L_{LNlung}\right) \\ \times (H(T_{LNlung}^{th} - T_{LNlung}^{ins})\ fi_{t,LNtumor} + H(T_{LNlung}^{ins} - T_{LNlung}^{th}))T_{LNlung}^{ins} \end{pmatrix} / V_{LNlung}^{ins} \tag{8c}$$

$$P(A_{LNlung}^{ins}, T_{LNlung}^{ins}) = \rho_{LNlung}\ T_{LNlung}^{ins}\ V_{LNlung}^{ins}\ H_{(A_{LNlung}^{ins} - A^{th})}\ H_{(T_{LNlung}^{ins} + nTcell)}\ H_{(T_{LNlung}^{th} - T_{LNlung}^{ins})}$$

where the first term is the proliferation rate of T cells in antigen-positive LNs of lung, the second term is T cell flow from lymphatic flow of tissue into LNs, and the last term is the fraction of T cells that bypasses the LN and exits at the efferent lymphatic vessel. The proliferation rate of T cells is a function of antigen concentration in the LN, n T cell presence in the LN, and the level of effector T cells in the LN.

d) Antigen distribution in LNs of lung

Antigen enters/leaves the LN blood supply via blood flow (and can extravasate):

$$\frac{dA^b_{LNlung}}{dt} = \begin{pmatrix} (1-f_{lung})(Q_{lung}-L_{lung})\ A^b_{lung} \\ -\left((1-f_{lung})(Q_{lung}-L_{lung})-L_{LNlung}\right)A^b_{LNlung} \\ -J_{a,LNlung}\ A^b_{LNlung}\ V^b_{LNlung} \end{pmatrix} / V^b_{LNlung} \tag{9a}$$

Antigen enters the LN via lymph flow; it can leave the LN via lymph flow, and degrade:

$$\frac{dA^{ins}_{LNlung}}{dt} = \begin{pmatrix} J_{a,LNlung}\ A^b_{LNlung}\ V^b_{LNlung} + (1-ff_{lung})\ \ L_{lung}\ A^{ins}_{lung}\ fi_{a,lung} \\ -\left((1-ff_{lung})\ \ L_{lung}+L_{LNlung}\right)A^{ins}_{LNlung}\ fi_{a,LNlung} \\ -\varepsilon_{LNlung}\ A^{ins}_{LNlung}\ V^{ins}_{LNlung} \end{pmatrix} / V^{ins}_{LNlung} \tag{9b}$$

Liver, Spleen and Intestine

a) T-cell trafficking in blood vessels and interstitium of other organs, such as liver, intestine and spleen.

These organs have a connected network of LNs. We assume a common LN region for the abdominal LN to show this connectivity. The upstream blood flow can enter intestine, spleen and liver and after plasma filtration, the interstitial plasma flows of these three organs can collect into their common LN region.

For the liver

$$\frac{dT^b_{liver}}{dt} = \begin{pmatrix} f_{liver}\,(Q_{\text{int}estine}-L_{\text{int}estine})T^b_{\text{int}estine} + f_{liver}\,(Q_{spleen}-L_{spleen})T^b_{spleen} \\ +\ f_{liver}\,(Q_{liver}-Q_{\text{int}estine}-Q_{spleen}+L_{\text{int}estine}+L_{spleen})T^a_{Heart} \\ -(\,f_{liver}\ \ Q_{liver}-L_{liver})T^b_{liver} \\ -a_{liver}\ T^b_{liver}\ V^b_{liver} \\ +d_{liver}\ T^c_{liver}\ V^b_{liver} \end{pmatrix} / V^b_{liver} \tag{10a}$$

where the first and second terms are the flow of T cells from the outlet blood flows of intestine and spleen into the liver, the third term is the flow of T cells from the arterial blood into the liver; the fourth term is the flow of T cells out of the liver; the two last terms represent the binding of T cells to the liver endothelium and the detachment of T cells from the endothelium. In Eqs. 10b and 10c, the terms with the parameter *J* are transmigration of T cells into the liver interstitium.

$$\frac{dT^c_{liver}}{dt} = \left(\ a_{liver}\ T^b_{liver}\ V^b_{liver} - d_{liver}\ T^c_{liver}\ V^b_{liver} - J_{t,liver}\ T^c_{liver}\ V^b_{liver}\ \right) / V^b_{liver} \tag{10b}$$

$$\frac{dT_{liver}^{ins}}{dt} = \left(J_{t,liver}\, T_{liver}^{c}\, V_{liver}^{b} - L_{liver}\, T_{liver}^{ins}\, fi_{t,liver} \right) / V_{liver}^{ins} \tag{10c}$$

For the spleen

$$\frac{dT_{spleen}^{b}}{dt} = \begin{pmatrix} Q_{spleen}\, T_{Heart}^{v} - (Q_{spleen} - L_{spleen}) T_{spleen}^{b} \\ - a_{spleen}\, T_{spleen}^{b}\, V_{spleen}^{b} \\ + d_{spleen}\, T_{spleen}^{c}\, V_{spleen}^{b} \end{pmatrix} / V_{spleen}^{b} \tag{10d}$$

where the first term is the flow of T cells from the arterial blood into the spleen; the second term is the flow of T cells out of the spleen; the third term represents the binding of T cells to the spleen endothelium, and the last term is the detachment of cells from the endothelium. In Eqs. 10e and 10f, the terms with *J* are transmigration of T cells into the spleen interstitium. The second term in Eq.10f is the drainage of T cell by filtration from the spleen interstitium to lymphatic vessels.

$$\frac{dT_{spleen}^{c}}{dt} = \left(a_{spleen}\, T_{spleen}^{b}\, V_{spleen}^{b} - d_{spleen}\, T_{spleen}^{c}\, V_{spleen}^{b} - J_{t,spleen}\, T_{spleen}^{c}\, V_{spleen}^{b} \right) / V_{spleen}^{b} \tag{10e}$$

$$\frac{dT_{spleen}^{ins}}{dt} = \left(J_{t,spleen}\, T_{spleen}^{c}\, V_{spleen}^{b} - L_{spleen}\, T_{spleen}^{ins}\, fi_{t,spleen} \right) / V_{liver}^{ins} \tag{10f}$$

For the intestine

$$\frac{dT_{\mathrm{int}estine}^{b}}{dt} = \begin{pmatrix} Q_{\mathrm{int}estine}\, T_{Heart}^{v} - (Q_{\mathrm{int}estine} - L_{\mathrm{int}estine}) T_{\mathrm{int}estine}^{b} \\ - a_{\mathrm{int}estine}\, T_{\mathrm{int}estine}^{b}\, V_{\mathrm{int}estine}^{b} \\ + d_{\mathrm{int}estine}\, T_{\mathrm{int}estine}^{c}\, V_{\mathrm{int}estine}^{b} \end{pmatrix} / V_{\mathrm{int}estine}^{b} \tag{10g}$$

where the first term is the flow of T cells from the arterial blood into the intestine; the second term is the flow of T cells out of the intestine; the third term represents the binding of T cells to the intestine endothelium, and the last term is the detachment of T cells from the intestine endothelium. In Eqs. 10h and 10l, the terms with *J* are transmigration of T cells into the intestine interstitium. The second term in Eq.10h is the drainage of T cell by filtration from the intestine interstitium to lymphatic vessels.

$$\frac{dT_{\mathrm{int}estine}^{c}}{dt} = \begin{pmatrix} a_{\mathrm{int}estine}\, T_{\mathrm{int}estine}^{b}\, V_{\mathrm{int}estine}^{b} - d_{\mathrm{int}estine}\, T_{\mathrm{int}estine}^{c}\, V_{\mathrm{int}estine}^{b} \\ - J_{t,\mathrm{int}estine}\, T_{\mathrm{int}estine}^{c}\, V_{\mathrm{int}estine}^{b} \end{pmatrix} / V_{\mathrm{int}estine}^{b} \tag{10h}$$

$$\frac{dT_{\mathrm{int}estine}^{ins}}{dt} = \left(J_{t,\mathrm{int}estine}\, T_{\mathrm{int}estine}^{c}\, V_{\mathrm{int}estine}^{b} - L_{\mathrm{int}estine}\, T_{\mathrm{int}estine}^{ins}\, fi_{t,\mathrm{int}estine} \right) / V_{\mathrm{int}estine}^{ins} \tag{10l}$$

b) antigen distribution in blood vessels and interstitium of liver, spleen, and intestine

For the liver

$$\frac{dA^{b}_{liver}}{dt}=\begin{pmatrix} f_{liver}\ (Q_{intestine}-L_{intestine})\,A^{b}_{intestine}+f_{liver}\ (Q_{spleen}-L_{spleen})A^{b}_{spleen} \\ +\,f_{liver}\ (Q_{liver}-Q_{intestine}-Q_{spleen}+L_{intestine}+L_{spleen})A^{a}_{Heart} \\ -\left(f_{liver}\ Q_{liver}-L_{liver}\right)A^{b}_{liver}-J_{a,liver}\,A^{b}_{liver}\,V^{b}_{liver} \end{pmatrix}/V^{b}_{liver} \tag{11a}$$

where the first and second terms are the flow of antigen into the liver via the bloodstream passing from intestine and spleen, the third term is the antigen flow from the arterial flow of heart into liver, the fourth term is antigen leaving the liver via the outlet blood flow and the last term is the filtration of antigen from the blood into the tumor tissue. In Eqs. 11b-f, the terms with J represent transmigration, the terms with L and Q-L are the antigen flows out via lymphatic system and the outlet blood flow. The ε terms are natural decay of antigen.

$$\frac{dA^{ins}_{liver}}{dt}=\begin{pmatrix} J_{a,liver}\,A^{b}_{liver}\,V^{b}_{liver}-L_{liver}\,A^{ins}_{liver}\,f_{a,liver} \\ -\varepsilon_{liver}\,A^{ins}_{liver}\,V^{ins}_{liver} \end{pmatrix}/V^{ins}_{liver} \tag{11b}$$

For the spleen

$$\frac{dA^{b}_{spleen}}{dt}=\begin{pmatrix} Q_{spleen}\,A^{a}_{Heart}-(Q_{spleen}-L_{spleen})A^{b}_{spleen} \\ -J_{a,spleen}\,A^{b}_{spleen}\,V^{b}_{spleen} \end{pmatrix}/V^{b}_{spleen} \tag{11c}$$

$$\frac{dA^{ins}_{spleen}}{dt}=\begin{pmatrix} J_{a,spleen}\,A^{b}_{spleen}\,V^{b}_{spleen}-L_{spleen}\,A^{ins}_{spleen}\,f_{a,spleen} \\ -\varepsilon_{spleen}\,A^{ins}_{spleen}\,V^{ins}_{spleen} \end{pmatrix}/V^{ins}_{spleen} \tag{11d}$$

For the intestines

$$\frac{dA^{b}_{intestine}}{dt}=\begin{pmatrix} Q_{intestine}\,A^{a}_{Heart}-(Q_{intestine}-L_{intestine})A^{b}_{intestine} \\ -J_{a,intestine}\,A^{b}_{intestine}\,V^{b}_{intestine} \end{pmatrix}/V^{b}_{intestine} \tag{11e}$$

$$\frac{dA^{ins}_{intestine}}{dt}=\begin{pmatrix} J_{a,intestine}\,A^{b}_{intestine}\,V^{b}_{intestine}-L_{intestine}\,A^{ins}_{intestine}\,fi_{a,intestine} \\ -\varepsilon_{intestine}\,A^{ins}_{intestine}\,V^{ins}_{intestine} \end{pmatrix}/V^{ins}_{intestine} \tag{11f}$$

c) T-cell trafficking in the abdominal LNs (LN_Abd)

$$\frac{dT^{b}_{LN\_Abd}}{dt}=\begin{pmatrix} (1-f_{liver})(Q_{intestine}-L_{intestine})T^{b}_{intestine} \\ +(1-f_{liver})(Q_{spleen}-L_{spleen})T^{b}_{spleen} \\ +(1-f_{liver})\,(Q_{liver}-Q_{intestine}-Q_{spleen}+L_{intestine}+L_{spleen})T^{a}_{Heart} \\ -\left((1-f_{liver})\,Q_{liver}-L_{LN\_Abd}\right)T^{b}_{LN\_Abd} \end{pmatrix}/V^{b}_{LN\_Abd} \tag{12a}$$

where the first term is the T cell flow in LNs via blood flow of the intestine, the second term is the T cell flow in LNs via blood flow of the spleen, the third term is the T cell flow from outflow of blood into the liver, and the last term is the fraction of T cells that bypasses the LN and exits at the efferent lymphatic vessel.

$$\frac{dT^{ins}_{LN\_Abd}}{dt}=\left(\begin{array}{l} P(A^{ins}_{LN\_Abd},T^{ins}_{LN\_Abd}) \\ +(1-ff_{liver})\ L_{liver}\ T^{ins}_{liver}\ fi_{t,liver}+(1-ff_{liver})\ L_{\mathrm{int}estine}\ T^{ins}_{\mathrm{int}estine}\ fi_{t,\mathrm{int}estine} \\ +(1-ff_{liver})\ L_{spleen}\ T^{ins}_{spleen}\ fi_{t,spleen} \\ -\left((1-ff_{liver})\,L_{liver}+(1-ff_{liver})\,L_{\mathrm{int}estine}+(1-ff_{liver})\,L_{spleen}+L_{LN\_Abd}\right) \\ \quad\times(H(T^{th}_{LN\_Abd}-T^{ins}_{LN\_Abd})\ fi_{t,LN\_Abd}+H(T^{ins}_{LN\_Abd}-T^{th}_{LN\_Abd}))\,T^{ins}_{LN\_Abd} \end{array}\right)/V^{ins}_{LN\_Abd} \quad (12b)$$

$$P(A^{ins}_{LN\_Abd},T^{ins}_{LN\_Abd})=\rho_{LN\_Abd}\ T^{ins}_{LN\_Abd}\ V^{ins}_{LN\_Abd}\ H_{(A^{ins}_{LN\_Abd}-A^{th})}\ H_{(T^{ins}_{LN\_Abd}+nTcell)}\ H_{(T^{th}_{LN\_Abd}-T^{ins}_{LN\_Abd})}$$

where the first term is the proliferation rate of T cells in antigen-positive LNs, the second, third and fourth terms are T cell flow from lymphatic flow of tissue into LNs, and the last term is the fraction of T cells that bypasses the LN and exits at the efferent lymphatic vessel. The proliferation rate of T cells is a function of antigen concentration in the LN, n T cell presence in the LN, and the level of effector T cells in the LN.

d) Antigen distribution in LN of liver/spleen/intestines

$$\frac{dA^{b}_{LN\_Abd}}{dt}=\left(\begin{array}{l} (1-f_{liver})\,(Q_{\mathrm{int}estine}-L_{\mathrm{int}estine})\,A^{b}_{\mathrm{int}estine} \\ +(1-f_{liver})\,(Q_{spleen}-L_{spleen})\,A^{b}_{spleen} \\ +(1-f_{liver})\,(Q_{liver}-Q_{\mathrm{int}estine}-Q_{spleen}+L_{\mathrm{int}estine}+L_{spleen})\,A^{a}_{Heart} \\ -\left((1-f_{liver})\,Q_{liver}-L_{LN\_Abd}\right)A^{b}_{LN\_Abd} \\ -J_{a,LN\_Abd}\ A^{b}_{LN\_Abd}\ V^{b}_{LN\_Abd} \end{array}\right)/V^{b}_{LN\_Abd} \quad (13a)$$

where the first, second and third terms are the flow of antigen from the intestine, spleen and liver, to the LN; the fourth term is the flow of antigen in the exit blood stream, and the last term is the antigen that crosses the blood vessel to enter the LN. The mass balance for antigen within the liver/intestine/spleen draining lymph node tissue ($A^{ins}_{LNtumor}$) is:

$$\frac{dA^{ins}_{LN\_Abd}}{dt}=\left(\begin{array}{l} J_{a,LN\_Abd}\ A^{b}_{LN\_Abd}\ V^{b}_{LN\_Abd}+(1-ff_{liver})L_{liver}\ A^{ins}_{liver}\ fi_{a,liver} \\ (1-ff_{liver})L_{\mathrm{int}estine}\ A^{ins}_{\mathrm{int}estine}\ fi_{a,\mathrm{int}estine}+(1-ff_{liver})\,L_{spleen}\ A^{ins}_{spleen}\ fi_{a,spleen} \\ -\left((1-ff_{liver})L_{liver}+(1-ff_{liver})L_{spleen}+(1-ff_{liver})L_{\mathrm{int}estine}+L_{LN\_Abd}\right)A^{ins}_{LN\_Abd}\ fi_{a,LN\_Abd} \\ -\varepsilon_{LN\_Abd}\ A^{ins}_{LN\_Abd}\ V^{ins}_{LN\_Abd} \end{array}\right)/V^{ins}_{LN\_Abd} \quad (13b)$$

where the first term is antigen entering the LN from the blood supply; the second term is the flow of antigen with the lymph via the afferent lymphatic vessel; the third term represents the fraction of antigen that bypasses the LN and exits at the efferent lymphatic vessel. The last term is the degradation of antigen in the node.

a) T-cell trafficking in blood and interstitium of the *i*th organ, including skin, muscle, bone, brain and kidney:

$$\frac{dT_i^b}{dt} = \begin{pmatrix} f_i\ Q_i\ T_{Heart}^a - (f_i\ Q_i - L_i) T_i^b \\ -a_i\ T_i^b\ V_i^b \\ +d_i\ T_i^c\ V_i^b \end{pmatrix} / V_i^b \quad (14a)$$

where the first term is the flow of T cells from the arterial blood into the i^{th} organ; the second term is the flow of T cells out of the i^{th} organ; the third term represents the binding of T cells to the endothelium of i^{th} organ, and the last term is the detachment of cells from the endothelium. In Eqs. 14b and c, the terms with *J* are transmigration of T cells, and the term with *L* is the outflow of T cells via lymphatic flow:

$$\frac{dT_i^c}{dt} = \left(a_i\ T_i^b\ V_i^b - d_i\ T_i^c\ V_i^b - J_{t,i}\ T_i^c\ V_i^b \right) / V_i^b \quad (14b)$$

$$\frac{dT_i^{ins}}{dt} = \left(J_{t,i}\ T_i^c\ V_i^b - L_i\ T_i^{ins}\ fi_{t,i} \right) / V_i^{ins} \quad (14c)$$

b) Antigen distribution in blood vessels and interstitium

$$\frac{dA_i^b}{dt} = \left(f_i\ Q_i\ A_{Heart}^b - (f_i\ Q_i - L_i)\ A_i^b - J_{a,i}\ A_i^b\ V_i^b \right) / V_i^b \quad (15a)$$

$$\frac{dA_i^{ins}}{dt} = \left(J_{a,i}\ A_i^b\ V_i^b - L_i\ A_i^{ins}\ fi_{a,i} - \varepsilon_i\ A_i^{ins} V_i^{ins} \right) / V_i^{ins} \quad (15b)$$

where the first term of Eq. 15a is the flow of antigen from the arterial blood into the i^{th} organ; the second term is the flow of antigen out of the i^{th} organ via outlet venous blood flow; the third is transmigration of antigen. In Eq.15b, the second term is the outflow of antigen from interstitium and the last term is natural decay of antigen.

c) T-cell trafficking in the LN of the ith compartment including skin, muscle, bone, brain and kidney:

$$\frac{dT_{LNi}^b}{dt} = \begin{pmatrix} (1-f_i)\ Q_i\ T_{Heart}^a \\ -\left((1-f_i)\ Q_i - L_{LNi}\right) T_{LNi}^b \\ \end{pmatrix} / V_{LNi}^b \quad (16a)$$

The first term is T cell flow from heart into LNs of i^{th} organ and the second term is T cell leaving the LNs of i^{th} organ via outlet venous blood flow,

$$\frac{dT_{LNi}^{ins}}{dt}=\begin{pmatrix} P(A_{LNi}^{ins},T_{LNi}^{ins}) \\ +(1-ff_i)\,L_i\,T_i^{ins}\;fi_{t,i} \\ -\big((1-ff_i)\,L_i+L_{LNi}\big) \\ \quad\times(H(T_{LNi}^{th}-T_{LNi}^{ins})\;fi_{t,LNi}+H(T_{LNi}^{ins}-T_{LNi}^{th}))\,T_{LNi}^{ins} \end{pmatrix}/V_{LNtumor}^{ins} \tag{16b}$$

$$P(A_{LNi}^{ins},T_{LNi}^{ins})=\rho_{LNi}\;T_{LNi}^{ins}\;V_{LNi}^{ins}\;H_{(A_{LNi}^{ins}-A^{th})}\;H_{(T_{LNi}^{ins}+nTcell)}\;H_{(T_{LNi}^{th}-T_{LNi}^{ins})}$$

Where the first term is the proliferation of T cells in the LNs of i^{th} organ, the second term is T cells in the LNs from interstitial flow, the last term is T cell flow leaving the LNs via lymphatic flows.

d) Antigen distribution in LN of compartment *i*

$$\frac{dA_{LNi}^{b}}{dt}=\begin{pmatrix} (1-f_i)\;Q_i\;A_{Heart}^{a} \\ -\big((1-f_i)\;Q_i-L_{LNi}\big)\,A_{LNi}^{b} \\ -J_{a,LNi}\,A_{LNi}^{b}\,V_{LNi}^{b} \end{pmatrix}/V_{LNi}^{b} \tag{17a}$$

$$\frac{dA_{LNi}^{ins}}{dt}=\begin{pmatrix} J_{a,LNi}\,A_{LNi}^{b}\,V_{LNi}^{b} \\ +(1-ff_i)\,L_i\;A_i^{ins}\;fi_{a,i} \\ -\big((1-ff_i)\,L_i+L_{LNi}\big)\,A_{LNi}^{ins}\;fi_{a,LNi} \\ -\varepsilon_{LNi}\,A_{LNi}^{ins}\;V_{LNi}^{ins} \end{pmatrix}/V_{LNi}^{ins} \tag{17b}$$

In Eq.17a, the first term is antigen flow from the heart into the i^{th} organ, the second term is antigen out form the LNs, and the last term is transmigration. In Eq. 17b, the second term is antigen flow from interstitial flow, the third terms is outflow of antigen from the LNs to the circulation, and the last term is the natural decay of antigen.

Heart

a) T-cell recirculation in arterial and venous blood flows

$$\frac{dT_{Heart}^{a}}{dt}=\begin{pmatrix} f_{lung}\,(Q_{lung}-L_{lung})\,T_{lung}^{b} \\ -(Q_{liver}+L_{spleen}+L_{\text{int}estine}+Q_{kidney}+Q_{tumor} \\ +Q_{skin}+Q_{muscle}+Q_{bone}+Q_{brain})\,T_{Heart}^{a} \end{pmatrix}/V_{Heart}^{a} \tag{18a}$$

Where the first term is the T cell flow from lung to left ventricle of heart and the second term is the T cell flow leaving the left ventricle to distribute among different organs.

$$\frac{dT^{v}_{Heart}}{dt} = \begin{pmatrix} \left((1-f_{lung})(Q_{lung}-L_{lung})-L_{LNlung}\right)T^{b}_{LNlung} \\ +(f_{tumor}\,Q_{tumor}-L_{tumor})T^{b}_{tumor}+\left((1-f_{tumor})\,Q_{tumor}-L_{LNtumor}\right)T^{b}_{LNtumor} \\ +(f_{liver}\,Q_{liver}-L_{liver})T^{b}_{liver}+\left((1-f_{liver})\,Q_{liver}-L_{LNliver}\right)T^{b}_{LNliver} \\ +(f_{i}\,Q_{i}-L_{i})T^{b}_{i}+\left((1-f_{i})\,Q_{i}-L_{LNi}\right)T^{b}_{LNi} \\ +\left((1-ff_{tumor})L_{tumor}+L_{LNtumor}\right)T^{ins}_{LNtumor}\;fi_{t,LNtumor} \\ +\left((1-ff_{lung})L_{lung}+L_{LNlung}\right)T^{ins}_{LNlung}\;fi_{t,LNlung} \\ +\left((1-ff_{liver})L_{liver}+(1-ff_{intestine})L_{intestine}+(1-ff_{spleen})L_{spleen}+L_{LNliver}\right)T^{ins}_{LNliver}\;fi_{t,LNliver} \\ +\left((1-ff_{i})L_{i}+L_{LNi}\right)T^{ins}_{LNi}\;fi_{t,LNi} \\ +\left(ff_{tumor}\,L_{tumor}\right)T^{ins}_{tumor}\;fi_{t,tumor} \\ +\left(ff_{lung}\,L_{lung}\right)T^{ins}_{lung}\;fi_{t,lung} \\ +\left(ff_{liver}\,L_{liver}\right)T^{ins}_{liver}\;fi_{t,liver}+\left(ff_{intestine}\,L_{intestine}\right)T^{ins}_{intestine}\;fi_{t,intestine}+\left(ff_{spleen}\,L_{spleen}\right)T^{ins}_{spleen}\;fi_{t,spleen} \\ +\left(ff_{i}\,L_{i}\right)T^{ins}_{i}\;fi_{t,i} \\ -Q_{lung}T^{v}_{Heart} \end{pmatrix} / V^{v}_{Heart} \tag{18b}$$

Where all the positive terms are flow of T cells into venous flow of heart and the last term is collected T cell flow leaving the heart via right ventricle flow (inflow of lung).

b) Arterial and venous recirculation of antigen

$$\frac{dA^{a}_{Heart}}{dt} = \begin{pmatrix} f_{lung}\,(Q_{lung}-L_{lung})\,A^{b}_{lung} \\ -(Q_{liver}+L_{spleen}+L_{intestine}+Q_{kidney}+Q_{tumor} \\ +Q_{skin}+Q_{muscle}+Q_{bone}+Q_{brain})\,A^{a}_{Heart} \end{pmatrix} / V^{a}_{Heart} \tag{19a}$$

Where the first term is the antigen flow from lung to left ventricle of heart and the second term is the antigen flow leaving the left ventricle to distribute among different organs.

$$\frac{dA^{v}_{Heart}}{dt} = \left(\begin{array}{l} \left((1-f_{lung})(Q_{lung}-L_{lung})-L_{LNlung}\right)A^{b}_{LNlung} \\ +(f_{tumor}\,Q_{tumor}-L_{tumor})\,A^{b}_{tumor}+\left((1-f_{tumor})\,Q_{tumor}-L_{LNtumor}\right)A^{b}_{LNtumor} \\ +(f_{liver}\,Q_{liver}-L_{liver})\,A^{b}_{liver}+\left((1-f_{liver})\,Q_{liver}-L_{LNliver}\right)A^{b}_{LNliver} \\ +(f_{i}\,Q_{i}-L_{i})\,A^{b}_{i}+\left((1-f_{i})\,Q_{i}-L_{LNi}\right)A^{b}_{LNi} \\ +\left((1-ff_{tumor})\,L_{tumor}+L_{LNtumor}\right)A^{ins}_{LNtumor}\;fi_{t,LNtumor} \\ +\left((1-ff_{lung})L_{lung}+L_{LNlung}\right)A^{ins}_{LNlung}\;fi_{t,LNlung} \\ +\left((1-ff_{liver})L_{liver}+(1-ff_{intestine})L_{intestine}+(1-ff_{spleen})L_{spleen}+L_{LNliver}\right)A^{ins}_{LNliver}\;fi_{t,LNliver} \\ +\left((1-ff_{i})\,L_{i}+L_{LNi}\right)A^{ins}_{LNi}\;fi_{t,LNi} \\ +\left(ff_{tumor}\,L_{tumor}\right)A^{ins}_{tumor}\;fi_{t,tumor} \\ +\left(ff_{lung}\,L_{lung}\right)A^{ins}_{lung}\;fi_{t,lung} \\ +\left(ff_{liver}\,L_{liver}\right)A^{ins}_{liver}\;fi_{t,liver}+\left(ff_{intestine}\,L_{intestine}\right)A^{ins}_{intestine}\;fi_{t,intestine}+\left(ff_{spleen}\,L_{spleen}\right)A^{ins}_{spleen}\;fi_{t,spleen} \\ +\left(ff_{i}\,L_{i}\right)A^{ins}_{i}\;fi_{t,i} \\ -Q_{lung}A^{v}_{Heart} \end{array} \right) / V^{v}_{Heart} \qquad (19b)$$

Where all the positive terms are the flows of antigen into venous flow of heart and the last term is the collected antigen flow leaving the heart via right ventricle flow (inflow of lung).

c) Mass conservation equations

$$f_{lung}\;Q_{lung} = f_{lung}\;L_{lung}+Q_{heart-to-liver}+Q_{spleen}+Q_{intestine}+Q_{kidney}+Q_{tumor} + Q_{skin}+Q_{muscle}+Q_{bone}+Q_{brain} \qquad (20a)$$

$$Q_{liver} = Q_{heart-to-liver}+(Q_{spleen}-L_{spleen})+(Q_{intestine}-L_{intestine}) \qquad (20b)$$

Model validation

To compare the model predictions with clinical observations, we simulated radiation therapy (RT) for six patients and measured tumor growth (Fig. 9S). Figs. 9S A-C are lung cancer patients treated with RT (2Gy, administered every day except weekends), and Figs. 9S D-F show cervical cancer patients with the same RT schedule. For each patient, the growth rate of tumor and the constant values of the linear-quadratic model of RT are assigned based on the experimental data. According to these results, the model can reproduce the tumor size reduction of different patients treated with RT, if we use the correct patient-specific parameters.

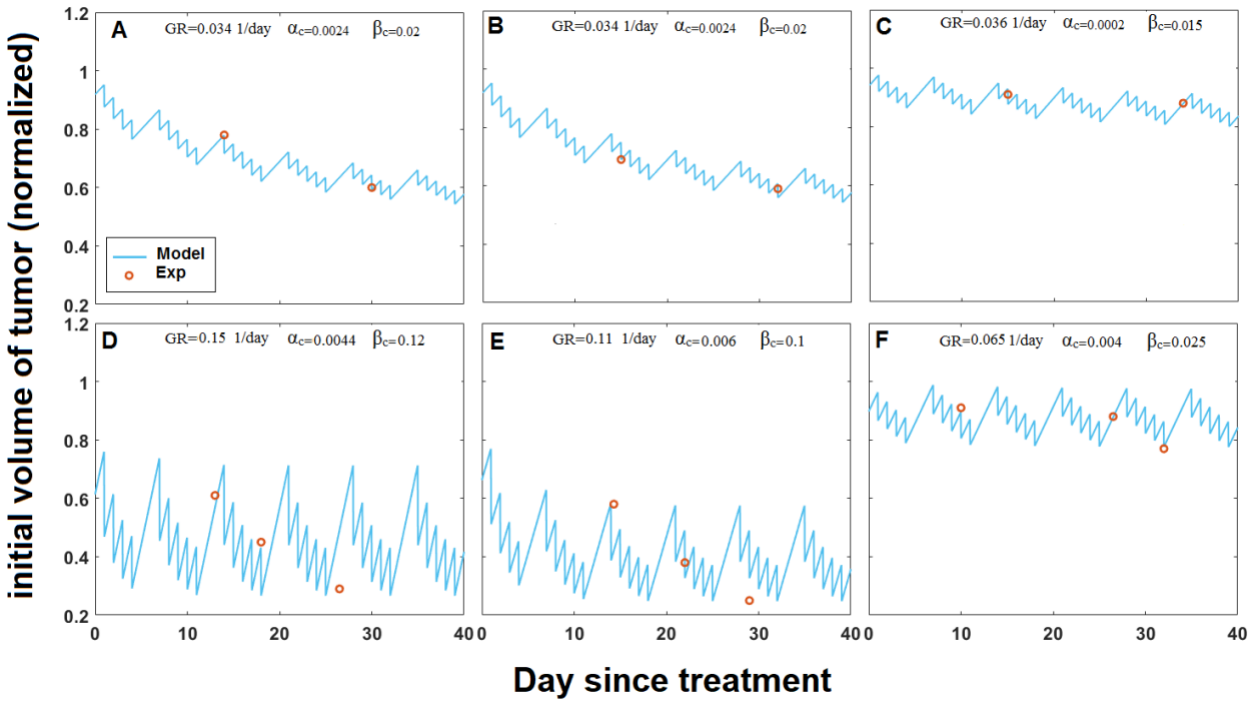

Figure S9. Comparison between model prediction and clinical results of tumor size reduction by RT with 2 Gy, injected daily for 5 days a week, A-B) lung cancer patients under RT with 2Gy, D-F) cervical cancer patients under RT with 2Gy.

Table S1. Model parameters

T-cell Transvascular	Description	constant	Ref
$J_{t,tumor}$	Transvascular migration rate of captured T cell into tumor tissue	2.1×10^{-4} min^{-1}	[4,5]
$J_{t,LNtumor}$	Transvascular migration rate of captured T cell into tumor LN	2.1×10^{-4} min^{-1}	[4,5]
$J_{t,i}$	Transvascular migration rate of captured T cell into i^{th} tissues; i = lung, liver, intestine, spleen, and the rest of i^{th} tissues	2.1×10^{-4} min^{-1}	[4,5]
Antigen Transvascular	**Description**	**constant**	**Ref**
$J_{a,tumor}$	Transvascular filtration rate of antigen into tumor tissue	0.43 1/d	Estimated
$J_{a,LNtumor}$	Transvascular filtration rate of antigen into tumor LN	0.21 1/d	Estimated
$J_{a,i}$	Transvascular filtration rate of antigen into i^{th} tissues; i = lung, liver, intestine, spleen, and the rest of i^{th} tissues	0.114 1/d	Estimated
$J_{a,LNi}$	Transvascular filtration rate of antigen into i^{th} LNs; i = lung, abdominal, and the rest of i^{th} LNs	0.114 1/d	Estimated
T cell adhesion	**Description**	**constant**	**Ref**
a_{tumor}	Constant attachment rate constant of T cell to the blood vessel wall of tumor ; Variable attachment rate of tumor: $a'_{tumor} = a_{tumor}(V/(1+V))$, V : *tumor volume*	6.9×10^{-3} min^{-1}	[4]
a_{lung}	Attachment rate of T cell to the blood vessel wall in lung	3.1×10^{-6} min^{-1}	[4]

a_{liver}	Attachment rate of T cell to the blood vessel wall in liver	7.6×10^{-9} min^{-1}	[4]
a_{spleen}	Attachment rate of T cell to the blood vessel wall in spleen	8.1×10^{-6} min^{-1}	[4]
$a_{intestine}$	Attachment rate of T cell to the blood vessel wall in intestine	8.1×10^{-6} min^{-1}	[4]
d_j	detachment rate of T cell from the blood vessel wall of all tissues	200 min^{-1}	[6,7]
Antigen natural decay	Description	constant	Ref
ε_{tumor}	Antigen natural decay rate in tissues and LNs interstitium	0.015 1/d	Estimated
Blood flow rate	Description	constant	Ref
Q_{tumor}	Initial Blood flow rate of tumor	0.564 [ml/min]	[4]
Q_{skin}	Blood flow rate of skin	220 [ml/min]	[4]
Q_{muscle}	Blood flow rate of muscle	413 [ml/min]	[4]
Q_{bone}	Blood flow rate of bone	138 [ml/min]	[8]
Q_{liver}	Blood flow rate of liver (hepatic portal vein from G.I. and spleen, and hepatic artery)	800 [ml/min]	[8]
Q_{spleen}	Blood flow rate of spleen	138 [ml/min]	[8]
$Q_{intestine}$	Blood flow rate of intestine	468 [ml/min]	[8]
Q_{kidney}	Blood flow rate of kidney	630 [ml/min]	[8]
Q_{brain}	Blood flow rate of brain	300 [ml/min]	Estimate - [8]
$Q_{cardic\ vessels}$	Blood flow rate of cardiac vessels	120 [ml/min]	Estimate - [8]
Lymphatic flow rate	Description	constant	Ref
L_{tumor}	Lymphatic flow rate of tumor	$3x10^{-2}$ [ml/min]	[4]
L_{liver}	Lymphatic flow rate of liver	$8.7x10^{-2}$ [ml/min]	[8]
L_{spleen}	Lymphatic flow rate of spleen	$8.7x10^{-4}$ [ml/min]	[8]
$L_{intestine}$	Lymphatic flow rate of intestine	3.0×10^{-1} [ml/min]	[8]
L_{kidney}	Lymphatic flow rate of kidney	$1x\ 10^{-3}$ [ml/min]	Estimate - [8]
L_{brain}	Lymphatic flow rate of brain	$1x\ 10^{-3}$ [ml/min]	Estimate - [8]
$L_{cardic\ vessels}$	Lymphatic flow rate of cardiac vessels	$4.3x\ 10^{-3}$ [ml/min]	Estimate - [8]
L_{Hlung}	Lymphatic flow rate of lung	$4.3x\ 10^{-2}$ [ml/min]	[8]
L_{LNj}	Lymphatic flow rate of LNs	$7.7x10^{-1}$ [ml/min]	[4]
Blood and lymphatic flow fraction	Description	constant	Ref
f_j	Fractional flow rate of blood into tumor tissue	0.995, 0.99, 0.95, 0.9	Estimated

ff_j	Fractional rate of lymphatic flow from tissue part to the main lymphatic flow	0.99	Estimated
T cell fraction from interstitium to lymphatic flow	Description	constant	Ref
$f_{t,j}$	T cell fraction from tissue interstitium of all compartments except tumor to lymphatic flow	1	[9]
$f_{t,tumor}$	T cell fraction from tissue interstitium of tumor to lymphatic flow	0	[9]
$f_{t,LNj}$	T cell fraction from LNs interstitium to lymphatic flow	0.018	[9]
Antigen fraction from interstitium to lymphatic flow	Description	constant	Ref
$f_{a,j}$	Antigen fraction from tissue interstitium of all compartments to lymphatic flow	1	Estimate-[9]
$f_{a,LNj}$	Antigen fraction from LNs interstitium to lymphatic flow	0.18	Estimate-[9]
Volume of tissue interstitium	Description	constant	Ref
V^{ins}_{tumor}	Averaged interstitium volume of tumor	10.9 [ml]	[4]
V^{ins}_{liver}	Averaged interstitium volume of liver	361.8 [ml]	[8]
V^{ins}_{spleen}	Averaged interstitium volume of spleen	34.7 [ml]	[8]
$V^{ins}_{intestine}$	Averaged interstitium volume of intestine	373.2 [ml]	[8]
V^{ins}_{kidney}	Averaged interstitium volume of kidney	96.6 [ml]	[8]
V^{ins}_{brain}	Averaged interstitium volume of brain	279 [ml]	Estimate
$V^{ins}_{cardic\ vessels}$	Averaged interstitium volume of cardiac vessels	42.9 [ml]	Estimate
V^{ins}_{lung}	Averaged interstitium volume of normal part of lung	299.7 [ml]	[8]
V^{ins}_{bone}	Averaged interstitium volume of bone	279 [ml]	[8]
V^{ins}_{muscle}	Averaged interstitium volume of muscle	4558 [ml]	[8]
V^{ins}_{skin}	Averaged interstitium volume of skin	227 [ml]	[8]
Volume of LN interstitium	Description	constant	Ref
V^{ins}_{LNs}	Averaged interstitium volume of LNs	34.7 [ml]	[4]
Volume of vascular tissue	Description	constant	Ref
V^{b}_{tumor}	Averaged vascular volume of tumor	1.4 [ml]	[4]
V^{b}_{liver}	Averaged vascular volume of liver	180.9 [ml]	[8]
V^{b}_{spleen}	Averaged vascular volume of spleen	17 [ml]	[8]
$V^{b}_{intestine}$	Averaged vascular volume of intestine	43 [ml]	[8]
V^{b}_{kidney}	Averaged vascular volume of kidney	28.4 [ml]	[8]
V^{b}_{brain}	Averaged vascular volume of brain	150 [ml]	Estimate
V^{a}_{Heart}	Averaged volume of arterial cardiac vessels	69.9 [ml]	Estimate

V^{v}_{Heart}	Averaged volume of venus cardiac vessels	60.6 [ml]	Estimate
V^{b}_{lung}	Averaged vascular volume of normal part of lung	99.9 [ml]	[8]
V^{b}_{bone}	Averaged vascular volume of bone	150 [ml]	[8]
V^{b}_{muscle}	Averaged vascular volume of muscle	700 [ml]	[8]
V^{b}_{skin}	Averaged vascular volume of skin	462 [ml]	[8]
Volume of vascular LN	Description	constant	Ref
$V^{b}_{LNtumor}$	Averaged vascular volume of LNs	17 [ml]	[4]
Antigen-induced T cell proliferation	Description	constant	Ref
ρ_{LNj}	T cell proliferation rate in LNs	1.4×10^{-3} min^{-1}	Estimated
A^{th}	Minimum antigen concentration for T cell proliferation	1.4×10^{-3} [1/ml]	Estimated
T^{th}_{LNj}	T cell capacity of LNs	1×10^{3} [1/ml]	Estimated
a_c	Production rate of antigen by cancer cells	Low-antigen: 1×10^{-5} min^{-1} High-antigen: 7×10^{-3} min^{-1}	Estimated
$a_{c,I}$	Production rate of antigen by immune-induced apoptotic cancer cells	Low-antigen: 3×10^{-5} min^{-1} High-antigen: 2.1×10^{-2} min^{-1}	Estimated
$a_{c,RT}$	Production rate of antigen by radiation-induced apoptotic cancer cells	Low-antigen: 3×10^{-3} min^{-1} High-antigen: 2.1×10^{-2} min^{-1}	Estimated
Radiotherapy model	Description	constant	Ref
ξ_c	Scale factor for the radiosensitivity of cancer cells	1	[10]
α_c	cell type-specific radiosensitivity parameters for cancer cells	0.3	[10]
β_c	cell type-specific radiosensitivity parameters for cancer cells	0.03	[10]
ξ_v	Scale factor for the radiosensitivity of endothelial cells	1	[10]
α_v	cell type-specific radiosensitivity parameters for endothelial cells	0.215	[10]
β_v	cell type-specific radiosensitivity parameters for endothelial cells	0.028	[10]
ξ_T	Scale factor for the radiosensitivity of T cells	1	[10]
α_T	cell type-specific radiosensitivity parameters for T cells	0.205	[10]
β_T	cell type-specific radiosensitivity parameters for T cells	0.025	[10]
$\varepsilon_{ap,RT}$	Decay rate of RT-killed cancer, vessels, and T cells	1×10^{-3} min^{-1}	Estimated
Tumor-immune interaction	Description	constant	Ref
k_1	T cell /tumor cell complex formation rate		[11]

		1.3 $\times 10^{-7}$ day^{-1} $(cell/ml)^{-1}$	
k_{-1}	T cell /tumor cell complex degeneration rate	24 day^{-1}	[11]
k_2	T cell/tumor cell complex stabilization rate	7.2 day^{-1}	[11]
p_r	PD-L1/PD-1 blockade efficiency	0.9997	Estimated- [11]
β_v	maximum value to enhance the accessibility of T cells to tumor cells by angiogenic vessels	10	Estimated- [11]
α_v	M-M constant to enhance the accessibility of T cells to tumor cells by angiogenic vessels	1	[11]
Tumor growth and Angiogenesis	Description	constant	Ref
g_v	Maximum rate of vascular tumor growth	1.4×10^{-3} min^{-1}	Estimated - [12,13]
g_{av}	Maximum rate of avascular tumor growth	7×10^{-7} min^{-1}	Estimated - [12,13]
λ_{a0}	M-M constant for Maximum avascular tumor growth	1	Estimated - [12,13]
η_{ag}	Production rate of tumor-induced VEGF	1.1×10^{-10} min^{-1}	Estimated- [14,15]
ε_{vegf}	Natural decay rate of tumor-induced VEGF	7×10^{-5} min^{-1}	Estimated- [14,15]
β_{ag}	Maximum rate of angiogenesis	1.4×10^{-4} min^{-1}	Estimated- [14,15]
$\alpha_{vegf\,0}$	M-M constant of angiogenesis rate	1×10^{-6}	Estimated- [14,15]
ω_{ag}	Maximum value of angiogenic vessel degradation	3.3×10^{-3} min^{-1}	Estimated- [14,15]
$\theta_{vegf\,0}$	M-M constant of angiogenic vessel degradation	3.3×10^{-7}	Estimated- [14,15]
residence time	Description	constant	Ref
tr_{LN}	Residence time of n T cells in LNs	10 hrs	[1,16]
tr_{spleen}	Residence time of n T cells in spleen	2.5 hrs	[1,16]
tr_{lung}	Residence time of n T cells in lung	0.46 min	[1,16]
tr_{liver}	Residence time of n T cells in liver	0.88 min	[1,16]
tr_i	Residence time of n T cells in other organs	0.21 min	Estimated, [1,16]

References

1 Ganusov, V. V. & Auerbach, J. Mathematical modeling reveals kinetics of lymphocyte recirculation in the whole organism. *PLoS computational biology* **10**, e1003586 (2014).

2 du Bois, H., Heim, T. A. & Lund, A. W. Tumor-draining lymph nodes: At the crossroads of metastasis and immunity. *Science immunology* **6**, eabg3551 (2021).

3 McMahon, S. J. The linear quadratic model: usage, interpretation and challenges. *Physics in Medicine & Biology* **64**, 01TR01 (2018).

4 Zhu, H., Melder, R. J., Baxter, L. T. & Jain, R. K. Physiologically based kinetic model of effector cell biodistribution in mammals: implications for adoptive immunotherapy. *Cancer research* **56**, 3771-3781 (1996).

5 Friedrich, S. W. *et al.* Antibody-directed effector cell therapy of tumors: analysis and optimization using a physiologically based pharmacokinetic model. *Neoplasia* **4**, 449-463 (2002).

6 Melder, R. J., Salehi, H. A. & Jain, R. K. Interaction of activated natural killer cells with normal and tumor vessels in cranial windows in mice. *Microvascular research* **50**, 35-44 (1995).

7 Bjerknes, M., Cheng, H. & Ottaway, C. A. Dynamics of lymphocyte-endothelial interactions in vivo. *Science* **231**, 402-405 (1986).

8 Zhu, H., Melder, R. J., Baxter, L. T. & Jain, R. K. Physiologically based kinetic model of effector cell biodistribution in mammals: implications for adoptive immunotherapy. *Cancer Res* **56**, 3771-3781 (1996).

9 Butcher, E. Following cellular traffic: methods of labelling lymphocytes and other cells to trace their migration in vivo. *Handbook of experimental immunology* **2**, 57.51 (1986).

10 Alfonso, J. C. *et al.* Tumor-immune ecosystem dynamics define an individual Radiation Immune Score to predict pan-cancer radiocurability. *Neoplasia* **23**, 1110-1122 (2021).

11 Matzavinos, A., Chaplain, M. A. & Kuznetsov, V. A. Mathematical modelling of the spatio-temporal response of cytotoxic T-lymphocytes to a solid tumour. *Mathematical Medicine and Biology* **21**, 1-34 (2004).

12 Watanabe, Y., Dahlman, E. L., Leder, K. Z. & Hui, S. K. A mathematical model of tumor growth and its response to single irradiation. *Theoretical Biology and Medical Modelling* **13**, 1-20 (2016).

13 Enderling, H. & AJ Chaplain, M. Mathematical modeling of tumor growth and treatment. *Current pharmaceutical design* **20**, 4934-4940 (2014).

14 Nikmaneshi, M. R., Firoozabadi, B., Mozafari, A. & Munn, L. L. A multi-scale model for determining the effects of pathophysiology and metabolic disorders on tumor growth. *Scientific reports* **10**, 1-20 (2020).

15 Nikmaneshi, M. R., Firoozabadi, B. & Mozafari, A. Chemo-Mechanistic multi-scale model of a three-dimensional tumor microenvironment to quantify chemotherapy response of cancer. *Biotechnology and Bioengineering* (2021).

16 Breart, B. & Bousso, P. S1P1 downregulation tailors CD8+ T-cell residence time in lymph nodes to the strength of the antigenic stimulation. *European Journal of Immunology* **46**, 2730-2736 (2016).